Henry's Law Constants and Hydration Equilibrium Constants of *n*-Hexanal and Their Temperature Dependence as Determined by the Rectangular Pulse Method

Shuzo Kutsuna[1,*], Naoki Kaneyasu[1]

[1] National Institute of Advanced Industrial Science and Technology (AIST)

16-1 Onogawa, Tsukuba, Ibaraki 305-8569, JAPAN

*Corresponding author: s-kutsuna@aist.go.jp

HIGHLIGHTS

• A stimulus–response experiment using a gas–liquid contactor was conducted.

• Change of a rectangular input pulse after passing through the contactor was examined.

• Henry's law and hydration equilibrium constants of *n*-hexanal were determined.

• Temperature dependence of constants was determined at 5.3–22.5 °C.

• Values for toluene, ethyl acetate, and ethyl trifluoroacetate were also determined.

ABSTRACT

The Henry's law constants of *n*-hexanal are needed to predict its rate of mass transfer between gas and aqueous phases. However, information on these constants is limited because the mass transfer of *n*-hexanal involves a reversible hydration reaction in water; therefore, Henry's law constants are difficult to obtain experimentally and cannot be deduced only from the gas-to-water equilibrium. Here, we conducted stimulus–response experiments using a rectangular input pulse and a double-mixing gas–liquid contactor to simultaneously determine Henry's law constants and hydration equilibrium constants for *n*-hexanal in deionized water, aqueous sodium chloride, or aqueous sodium sulfate in the temperature range of 5.3–22.5 °C. The change in the concentration of a mixture of *n*-hexanal in nitrogen gas after passing through the contactor was examined, and simulation-based optimization was conducted to optimize parameters that included Henry's law constants and hydration rate constants. In the simulation, convolution using the rectangular input pulse was used to determine the input signal, and perfect gas-phase mixing and two-film layer mass transfer were assumed. This approach, which we called the rectangular pulse method, was validated by performing similar investigations for toluene, ethyl acetate, and ethyl trifluoroacetate. As a result, Henry's law constants and rate constants for the reversible hydration reactions of *n*-hexanal and their temperature dependence were obtained, and the calculated effective Henry's law constant agreed with some, but not all, of the values reported in the literature. A potential reason for the disagreement was discussed

from the viewpoint of long time-constants used for the hydration equilibrium. In addition, a salting effect by the aqueous salt solutions was found to affect the Henry's law constants, but not the hydration equilibrium constants. The overall liquid-side mass-transfer coefficient was found to be correlated with the diffusion coefficient, based on the Higbie penetration theory.

GRAPHICAL ABSTRACT

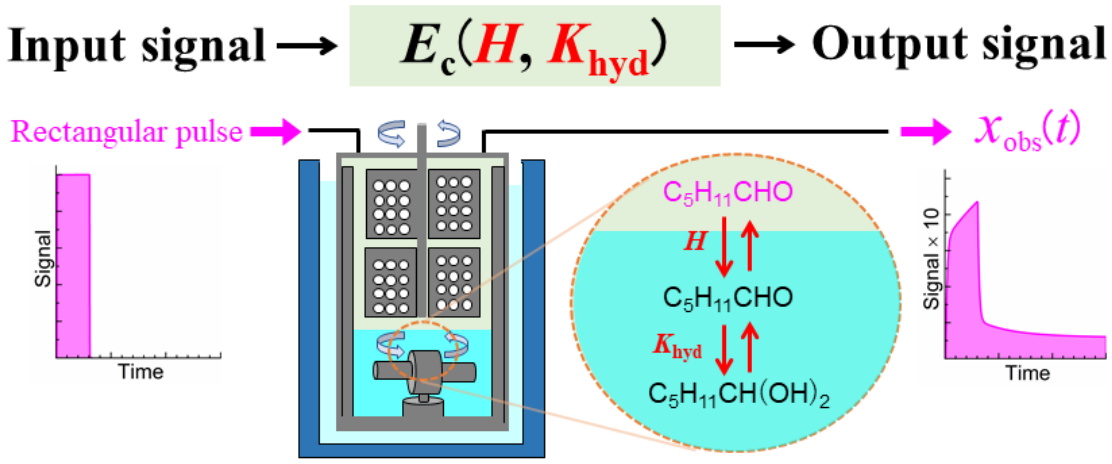

KEYWORDS

Aldehyde, Geminal Diol, Two-film Layer, Mass transfer, Residence Time Distribution, Salting Effect

1. INTRODUCTION

n-Hexanal ($C_5H_{11}CHO$) is an aliphatic aldehyde (RCHO) and common in the atmosphere, released directly from natural and anthropogenic sources such as forests, pastures, and vehicles (Brilli et al., 2012; Ervens and Kreidenweis, 2007; Tang and Zhu, 2004; Winer et al., 1992). It is also produced by atmospheric reactions such as gas-phase ozonolysis of alkenes (Atkinson et al., 1995) and heterogeneous oxidation of polyunsaturated fatty acids at air–water interfaces

such as the sea surface microlayer (Zhou et al., 2014). Like other aliphatic aldehydes (RCHOs), *n*-hexanal is a precursor of photooxidants such as peroxyacyl nitrates (Grosjean et al., 1996). *n*-Hexanal is also an aroma compound found in commercial food products (Buttery et al., 1969). Release of aroma compounds from these products is of great importance for the optimization of food processing techniques and for understanding food properties such as flavor and aging (Karl et al., 2003). To predict the atmospheric behavior of *n*-hexanal and its release from food products, accurate rates of mass transfer between gas and aqueous phases are needed, the calculation of which depends on the Henry's law constant (H, in M atm^{-1}). However, information on the values of H for *n*-hexanal and other RCHOs is limited.

Because aqueous RCHOs undergo a reversible hydration reaction to form the corresponding hydrate, $RCH(OH)_2$ (geminal diol) (Eq. 1), the gas-to-water equilibrium is described not only by the value of H (Eq. 2) but also by the value of the hydration equilibrium constant (K_{hyd}) (Eq. 3). Therefore, for RCHOs, the effective Henry's law constant (H^*, in M atm^{-1}) is used to describe the equilibrium distribution and the direction of mass transfer between the gas and aqueous phases. Thus,

$$\mathrm{RCHO} + \mathrm{H_2O} \rightleftarrows \mathrm{RCH(OH)_2} \quad (1)$$

$$H = \frac{[\mathrm{RCHO}]_{eq}}{P_{\mathrm{RCHO}}} \quad (2)$$

$$K_{hyd} = \frac{[\mathrm{RCH(OH)_2}]_{eq}}{[\mathrm{RCHO}]_{eq}} \quad (3)$$

$$H^* = \frac{[\mathrm{RCHO}]_{eq} + [\mathrm{RCH(OH)_2}]_{eq}}{P_{\mathrm{RCHO}}} = H\left(1 + K_{hyd}\right) \quad (4)$$

where P_{RCHO} (in atm) is the partial pressure of the RCHO, and $[RCHO]_{eq}$ and $[RCH(OH)_2]_{eq}$ are the aqueous-phase equilibrium concentrations (in M) of RCHO and $RCH(OH)_2$, respectively.

Experimental determination of H values is more difficult than that of H^* values because H^* values can be deduced directly from the gas-to-water equilibrium. Therefore, most gas-to-water equilibrium coefficients currently in the literature for RCHOs are values of H^* and information on the values of H and K_{hyd} is limited. However, values of H and K_{hyd} are needed to predict the rates of mass transfer between gas and aqueous phases and the aqueous reactions of RCHOs, respectively.

For *n*-hexanal, most gas-to-water equilibrium coefficients reported are values of H^*, and there is considerable variation in the reported values, and their temperature dependence varies by ca. 20 kJ mol^{-1} in terms of enthalpy of dissolution (Bruneel et al., 2016; Sander, 2015). Similarly, K_{hyd} values for *n*-hexanal based on nuclear magnetic resonance or near-ultraviolet spectroscopic measurements of aqueous species have been reported (Buschmann et al., 1982; Buschmann et al., 1980; Sham and Joens, 1995); however, the reported values differ by a factor of approximately 2. Thus, accurate values of H cannot be calculated from these H^* and K_{hyd} values. However, if the values of H or H^* and K_{hyd} could be determined simultaneously during a single experimental run, more-accurate values of H could be determined.

Here, we determined values of H and K_{hyd} for *n*-hexanal by using data from a single experiment. We assumed that these values could be determined if the mass-transfer rate and distribution between the gas and aqueous phases for a given system were known, because the mass-transfer rate of *n*-hexanal between these two phases is controlled mostly by the value of H because of

the small rate constant for the hydration of this compound, which is around 10^{-3} s^{-1} (Buschmann et al., 1982). To this end, we used a stimulus–response experimental approach to simultaneously measure mass-transfer rates and distributions of the test compound between gas and aqueous phases. In this approach, a gas mixture containing the test compound was introduced as a rectangular pulse into a gas–liquid contactor, and then the change in the concentration of the test compound in the gas mixture leaving the contactor was examined. Simulation-based optimization was used to optimize the parameters related to the mass transfer and distribution of the test compound between the two phases in the contactor. Together, we call this approach the rectangular pulse method.

Using this approach, we determined the values of H and K_{hyd} for *n*-hexanal in deionized water, 0.6 M aqueous sodium chloride (NaCl), and 0.2 M aqueous sodium sulfate (Na_2SO_4) in the temperature range of 5.3–22.5 °C. Mass transfer between the gas and aqueous phases and the aqueous-phase reversible hydration reactions of *n*-hexanal in the contactor were simulated to reproduce the concentration–time profile of *n*-hexanal in the gas mixture leaving the contactor. The simulation used the convolution of the residence time distributions of the inlet and outlet regions with the rectangular input pulse of *n*-hexanal as the input signal, and the convolution was determined experimentally as described in detail in Section 2.3.2. Perfect gas-phase mixing and two-film layer mass transfer between the two phases were assumed in the simulation. The applicability of assuming perfect gas-phase mixing was confirmed in an experiment using *n*-heptane (C_7H_{16}). To validate the rectangular pulse method, we also determined values of H for toluene ($C_6H_5CH_3$) and ethyl acetate ($CH_3COOC_2H_5$) in deionized water, and values of H and the hydrolysis rate constant (k_h, in s^{-1}) for ethyl trifluoroacetate ($CF_3COOC_2H_5$) in deionized water and 0.6 M aqueous NaCl.

2. MATERIALS AND METHODS

2.1 Materials

n-Hexanal (99.9%) and ethyl trifluoroacetate (99%) were purchased from Sigma-Aldrich. Toluene (99.8%), ethyl acetate (99.5%), *n*-heptane (>99%), sodium chloride (>99.5%), and sodium sulfate (>99%) were purchased from FUJIFILM Wako Chemical Co. These reagents were used without further purification. Water was purified with an EMD Millipore Milli-Q Gradient A10 system (>18 MΩ·cm).

2.2 Experimental setup and procedure for the rectangular pulse method

Figure 1 shows the experimental setup for the rectangular pulse method. Each experimental run comprised preparation of a gas mixture containing the test compound, passage of the mixture through a gas–liquid contactor, and analysis of the mixture leaving the gas–liquid contactor. Gas mixture injection and analysis were fully automated via a program developed in-house. The flow rates of the gas mixtures were controlled with mass-flow controllers of MFC1 (M-100, MKS Instruments, Inc.), MFC2 (M-100B, MKS Instruments, Inc.) and MFC3 (FCST 1005LC-4F2-F500-AIR, Fujikin, Co.).

Gas mixture preparation and injection into the contactor. A sample of the test compound was placed in a perfluoroalkoxy alkane (PFA) bottle enclosed in the cavity of the aluminum block of an electronic dry bath (CTU-Mini, Taitec Co.) set at 288.2 or 295.2 K (Figure 1, *a* and *b*). Then, N_2 was slowly bubbled through the test compound to produce a sample–N_2 mixture (*c*), after which the sample–N_2 mixture was further diluted with N_2 to produce a diluted gas mixture that is hereafter referred to as ‘SG-a’ (*d*). Next, SG-a was injected, via a computer-controlled precision syringe pump module (PSD/4, Hamilton Co.) comprising a 1.25×10^{-2} dm^3 glass

gas-tight syringe and a three-port ceramic valve (*e* and *f*), into a flow of N_2 gas that had been fully humidified at the same temperature as that of the contactor, resulting in a diluted sample–N_2 gas mixture that is hereafter referred to as 'SG-b'. The syringe pump introduced SG-b into the contactor as a rectangular pulse (pulse width, 300 s; partial pressure, 10^{-4} atm; total flow rate, 1.8×10^{-3} dm^3 s^{-1}). Table S1 summarizes the experimental conditions used for preparing SG-a and SG-b, and the concentration of the test compound in each gas. The concentration of each test compound in SG-a was estimated assuming that the N_2 gas passing through the test compound in the PFA bottle was saturated with the vapor of the test compound. Saturated vapor pressure values were obtained from the literature for *n*-heptane (Carruth and Kobayashi, 1973), toluene (Besley and Bottomley, 1974), ethyl acetate (Polák and Mertl, 1965), ethyl trifluoroacetate (Huang et al., 2015), and *n*-hexanal (Covarrubias-Cervantes et al., 2004).

Gas–liquid contactor. The contactor, a cylindrical PFA vessel (*l*) (No.0500 PFA jar, AS ONE), was almost fully submerged in a temperature-controlled (range, 278.5–295.7 K) jacketed stainless-steel water bath (BT-80, SGI) (*i* and *j*); the temperature was adjusted by circulating temperature-controlled water (F-12-ED, Julabo Japan Co., Ltd.) through the jacket. Inside the contactor, 0.180 dm^3 of deionized water or aqueous salt solution was placed, leaving a remaining gas-phase volume of 0.320 dm^3. A polytetrafluoroethylene (PTFE) coated, stainless-steel six-blade turbine (Yamazaki Seisakusyo Inc.) was used to stir the gas phase at 300 rpm (*m*). The six-blade turbine consisted of two sets of three-blades, arranged horizontally, with each blade containing 12 holes. The blades were rotated by an electric motor connected to the contactor via a magnetic seal joint (FMB-006-BFNN-EM-S1, Rigaku Mechatronics Co.). A cylindrical PTFE magnetic stirring bar with PTFE support and baffles (Tsukuba Hikari Kagaku Co., Ltd) and a magnetic stirrer (RCX-1000D, Eyela) were used to stir the aqueous phase at 200, 300, or 400 rpm (*n*, *p*). The rotation directions of the turbine and magnetic stirrer were the

same. To facilitate mixing, four PTFE-coated, stainless-steel baffles were also set in the contactor (*o*). Figure S1 shows the dimensions of the six-blade turbine, magnetic stirring bar, and baffles. In addition, N_2 was slowly introduced into the contactor (ca. 8×10^{-6} dm^3 s^{-1}) with a mass-flow controller (M-100, MKS Instruments, Inc.) through the dead space between the contactor and the axis of the six-blade turbine to prevent the sample gases from residing there. The other parts of the gas–liquid contactor, which included the PTFE top lid of the cylindrical vessel and the support for the electric motor connected to the contactor, were manufactured in the workshop of our institute. A four-port PTFE valve (*k*) was used to select whether or not SG-b passed through the contactor.

Detection and analysis. After passing through the contactor, part of the gas mixture was drawn to the sampling loop of a six-port valve (type ET2C6UWE; VICI Valco Instruments Co. Inc.) by a sampling pump (SP208Dual II, GL Sciences Inc.) at 1.5×10^{-2} dm^3 min^{-1} and at almost atmospheric pressure. The gas in the loop was sampled every 30 s, and changes in the partial pressure of the test compound over time were determined by gas chromatography (GC) on an instrument equipped with a flame ionization detector (FID) (GC-2014, Shimadzu Co.). The sampling loop (volume, 4.69×10^{-4} dm^3) was coated with Silcosteel and was heated to ca. 353 K. An Rtx-5 GC column (0.53 mm ID × 15 m; Restek Co.) was used to separate the test compound from the N_2 gas. A similar analysis was also conducted to determine the partial pressure of the test compound before the gas mixture was passed through the contactor. The GC conditions for each test compound are listed in Table S2. GC peak height was used to determine the ratio of the test compound passing through the contactor in the gas phase to that not passing through the contactor. This ratio is denoted as x_{obs}, as described in Section 2.3.2.

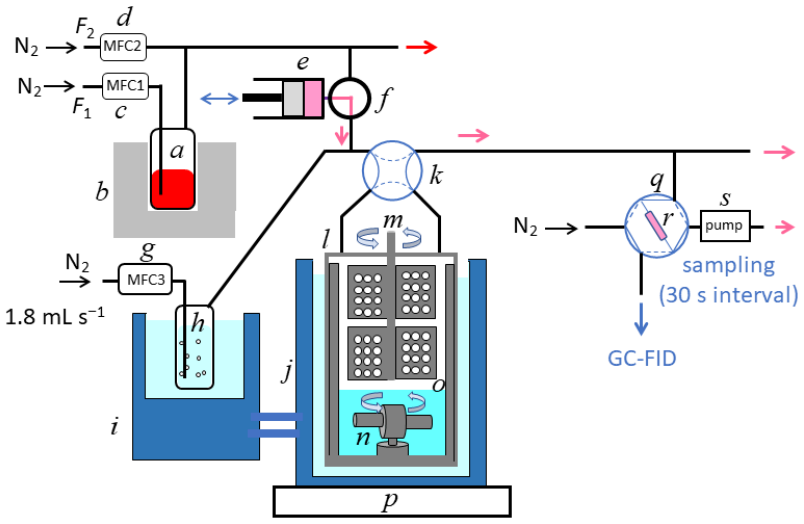

Figure 1. Setup for the rectangular pulse experiment. *Sample preparation and injection*: *a*, perfluoroalkoxy alkane bottle containing the test compound; *b*, electronic dry bath; *c* and *d*, mass-flow controllers; *e*, computer-controlled syringe pump; *f*, computer-controlled three-port ceramic valve; *g*, mass flow controller; *h*, humidifier; *i*, temperature-controlled water circulator. F_1 and F_2 are the N_2 gas flow rates controlled by mass-flow controllers 1 and 2 (MFC1 and MFC2), respectively. *Gas–liquid contactor*: *j*, jacketed stainless-steal water bath; *k*, four-port polytetrafluoroethylene (PTFE) valve; *l*, gas–liquid contactor; *m*, six-blade turbine for stirring the gas phase; *n*, PTFE magnetic bar for stirring the aqueous phase; *o*, baffles; *p*, magnetic stirrer. *Detection*: *q*, six-port valve for injecting samples into a gas chromatograph with flame ionization detector (GC-FID); *r*, sampling loop; *s*, pump for drawing the gas mixture into the sampling loop.

2.3 Parameter fitting to determine values of H *and rate constants for aqueous reactions*

2.3.1 Two-film layer theory and perfect gas-phase mixing

Letting $P_c(t)$ and $Q_c(t)$ be the partial pressure (in atm) and the mass (in mol), respectively, of the test compound in the gas mixture in the contactor at time t after injection by the syringe pump, the change of $Q_c(t)$ over time can be described by Eq. 5 on the basis of mass-balance

under the assumption of perfect gas-phase mixing. The boundary condition is $P_c(0) = 0$. Mass transfer between the gas and aqueous phases was treated as straight mass transfer in terms of the two-film layer theory (Lewis and Whitman, 1924). The validity of assuming perfect gas-phase mixing was checked as described in Section 2.3.3.

$$\frac{dQ_c(t)}{dt} = \frac{V_G}{RT}\frac{dP_c(t)}{dt} = \frac{F_G P_{in} f(t)}{RT_0} - E_L S_{GL} K_{MO} \times \left(HP_c(t) - C(t)\right) - \frac{F_G P_c(t)}{RT_0} \quad (5)$$

where $C(t)$ (in M or mol dm^{-3}) is the concentration of the test compound in the body of the liquid at time t; P_{in} (in atm) is the partial pressure of the rectangular input pulse, and $P_{in} f(t)$ is the time profile of the partial pressure of the rectangular input pulse; R is the gas constant; T and V_G are the temperature (in K) and gas-phase volume (3.20×10^{-1} dm^3) of the contactor, respectively; T_0 is 298.15 K; S_{GL} is the gas–liquid interface area (5.0×10^{-1} dm^2); K_{MO} (in dm s^{-1}) is the overall liquid-side mass-transfer coefficient from gas to liquid, and its negative value indicates mass transfer from liquid to gas; F_G (in dm^3 s^{-1} at T_0) is the total flow rate of the gas mixture passing through the contactor; and E_L is the liquid-film enhancement factor for mass transfer with aqueous reactions (Levenspiel, 1999; Lewis and Whitman, 1924). For the compounds examined in the present study, hydrolysis of ethyl trifluoroacetate and reversible hydration of *n*-hexanal occur in the aqueous phase, but the value of E_L was still set at 1. The assumption of $E_L = 1$ was judged to be appropriate, as described in Section 3.5. Rearranging Eq. 5 gives Eq. 6.

$$\frac{dP_c(t)}{dt} = \frac{F_G}{V_G}\frac{T}{T_0}P_{in} f(t) - \frac{RT}{V_G}E_L S_{GL} K_{MO} \times (HP_c(t) - C(t)) - \frac{F_G}{V_G}\frac{T}{T_0}P_c(t) \quad (6)$$

For each test compound, the aqueous-phase concentration and its change with time were

250 determined by the compound's aqueous reactions as follows:

251 For toluene and ethyl acetate,

252 $$\frac{\mathrm{d}C(t)}{\mathrm{d}t} = \frac{S_{\mathrm{GL}}K_{\mathrm{MO}}}{V_L} \times (HP_{\mathrm{c}}(t) - C(t)) \quad (7a)$$

253 For ethyl trifluoroacetate,

254 $$\frac{\mathrm{d}C(t)}{\mathrm{d}t} = \frac{S_{\mathrm{GL}}K_{\mathrm{MO}}}{V_L} \times (HP_{\mathrm{c}}(t) - C(t)) - k_{\mathrm{h}}C(t) \quad (7b)$$

255 For *n*-hexanal,

256 $$\frac{\mathrm{d}C(t)}{\mathrm{d}t} = \frac{S_{\mathrm{GL}}K_{\mathrm{MO}}}{V_L} \times (HP_{\mathrm{c}}(t) - C(t)) - k_{\mathrm{f}}C(t) + k_{\mathrm{b}}C_{\mathrm{diol}}(t) \quad (7c)$$

257 and $$\frac{\mathrm{d}C_{\mathrm{diol}}(t)}{\mathrm{d}t} = k_{\mathrm{f}}C(t) - k_{\mathrm{b}}C_{\mathrm{diol}}(t) \quad (7d)$$

258 Here, V_{L} is the aqueous-phase volume (1.80×10^{-1} dm^3); k_{h} (in s^{-1}) is the rate constant for the
259 hydrolysis of ethyl trifluoroacetate; k_{f} (in s^{-1}) and k_{b} (in s^{-1}) are the rate constants for the
260 hydration of *n*-hexanal and the backward reaction of the hydration, that is, the dehydration of
261 *n*-hexane-1,1-diol ($C_5H_{11}CH(OH)_2$), respectively; $C_{\mathrm{diol}}(t)$ is the aqueous concentration of *n*-
262 hexane-1,1-diol at time *t*. Values of K_{hyd} for *n*-hexanal were calculated from the values of k_{f}
263 and k_{b} by using Eq. 8:

264 $$K_{\mathrm{hyd}} = \frac{k_{\mathrm{f}}}{k_{\mathrm{b}}} \quad (8)$$

265

266 *2.3.2 Input signal and parameter fitting procedure in the simulation*

We simulated the partial pressure of the test compound in the gas mixture leaving the contactor by using a model in which the values of H, k_h, k_f, k_b, and other parameters were used as fitting parameters to best reproduce the observed ratios of the test compound passing through the contactor in the gas phase to that not passing through the contactor ($x_{obs}(t)$), which was defined as $P_{obs}(t)/P_{in\text{-}obs}$, where $P_{obs}(t)$ is the partial pressure measured at the GC-FID of the test compound in the gas mixture leaving the contactor at time t, and $P_{in\text{-}obs}$ is the partial pressure of the test compound in the rectangular input pulse measured at the GC-FID when the gas mixture did not pass through the contactor. Both values include measurement errors. Letting $P_{output}(t)$ be the partial pressure of the test compound with no measurement error, $x_{obs}(t)$ can be expressed as $\alpha_{corr} P_{output}(t)/P_{in}$, where the value of α_{corr} is the potential calibration error of $x_{obs}(t)$, which includes the errors for $P_{in\text{-}obs}$ and $P_{obs}(t)$. Values of α_{corr} were fitted as a parameter to reproduce the observed values.

The fitting was performed using the parameter-fitting routine of the FACSIMILE software (MCPA Software Ltd., UK), as described in detail elsewhere (Kutsuna, 2018). The simulation used $P_{in} f_{eq}(t)$, instead of $P_{in} f(t)$ in Eq. 6, as the input signal, where $P_{in} f_{eq}(t)$ is the convolution of the residence time distributions of inlet and outlet regions with the rectangular pulse, as described below (Levenspiel, 1999). This was because the input pulse was delayed and modified due to dispersion and adsorption of the gas mixture on the walls of the tubes as the mixture flowed from the syringe pump to the inlet of the contactor, which we defined as the "inlet region". $P_{output}(t)$ differed from P_c(t) for similar reasons as the gas mixture flowed from the outlet of the contactor to the GC-FID, which we defined as the "outlet region". The function of $f_{eq}(t)$ was determined experimentally based on RTD theory (Levenspiel, 1999).

Letting $E_{inlet}(t)$ be the RTD of the gas mixture passing through the inlet region and $E_c(t)$ be the

RTD of the gas mixture passing through the contactor, $P_c(t)$ can be presented as follows:

$$P_c(t) = \int_0^t \left\{ \int_0^{t'} P_{in} f(u) E_{inlet}(t' - u) du \right\} E_c(t - t') dt' \quad (9)$$

Because $E_{inlet}(t) = E_c(t) = 0$ for $t \leq 0$, Eq. 10 applies:

$$P_c(t) = \int_0^{\infty} \left\{ \int_0^{\infty} P_{in} f(u) E_{inlet}(t' - u) du \right\} E_c(t - t') dt' \quad (10)$$

From Eqs. 9 and 10, it can be inferred that $P_c(t)$ is the convolution of $E_c(t)$ with $\int_0^{\infty} P_{in} f(u) E_{inlet}(t' - u) du$, which is the convolution of $E_{inlet}(t)$ with $P_{in}\, f(t)$. As shown in Supplementary material, $E_c(t)$ does not change if the input signal is changed. Letting $E_{outlet}(t)$ be the RTD of the sample gas mixture passing through the outlet region, Eq. 10 gives Eq. 11 because convolution is commutative when $E_{outlet}(t) = f(t) = 0$ for $t \leq 0$. Here, the convolutions are indicated by $*$.

$$P_{output}(t) = P_c * E_{outlet} = P_{in} f * E_{inlet} * E_c * E_{outlet} = P_{in} f * E_{inlet} * E_{outlet} * E_c \quad (11)$$

Eq. 11 shows that $P_{output}(t)$ is the convolution of $E_c(t)$ with $P_{in}\, f(t) * E_{inlet} * E_{outlet}$. $P_{in}\, f(t) * E_{inlet} * E_{outlet}$ is therefore the input signal, $P_{in} f_{eq}(t)$, for estimating $E_c(t)$; $f_{eq}(t)$ is given by Eq. 12, and Eq. 11 can be rewritten as Eq. 13.

$$f_{eq}(t) = f * E_{inlet} * E_{outlet} \quad (12)$$

$$\frac{P_{output}(t)}{P_{in}} = \frac{1}{\alpha_{corr}} x_{obs}(t) = f_{eq} * E_c \quad (13)$$

$f_{eq}(t)$ was determined experimentally by connecting the inlet and outlet tubes of the contactor,

thus bypassing the contactor, and determining $x_{obs}(t)$ at every 30 s (Figure S2). The initial sampling time for the GC-FID measurement was delayed by a certain time period from the start of the sample injection by the syringe pump, and these measurements were repeated while the delay time was increased by 0.2 s. In this procedure, an injection pulse with a width of 120 s, rather than 300 s, was used to reduce the total run time. The time-profiles of the increase and decrease of $f_{eq}(t)$ are approximated by Eqs. 14 and 15, respectively:

$$f_{eq}(t) = \frac{1}{\left(1+\left(\frac{t}{a_1}\right)^{-a_2}\right)^{a_3}} \quad (14)$$

$$f_{eq}(t) = \frac{1}{\left(1+\left(\frac{t-300}{b_1}\right)^{-b_2}\right)^{b_3}} \quad (15)$$

where a_1, a_2, a_3, b_1, b_2, and b_3 are parameters determined from the experimental data by nonlinear regression. The experimental data are shown in Figures S3–S7. Table S3 lists the values of a_1, a_2, a_3, b_1, b_2, and b_3 determined for each test compound. Figure 2 shows parts of $f_{eq}(t)$ for each test compound.

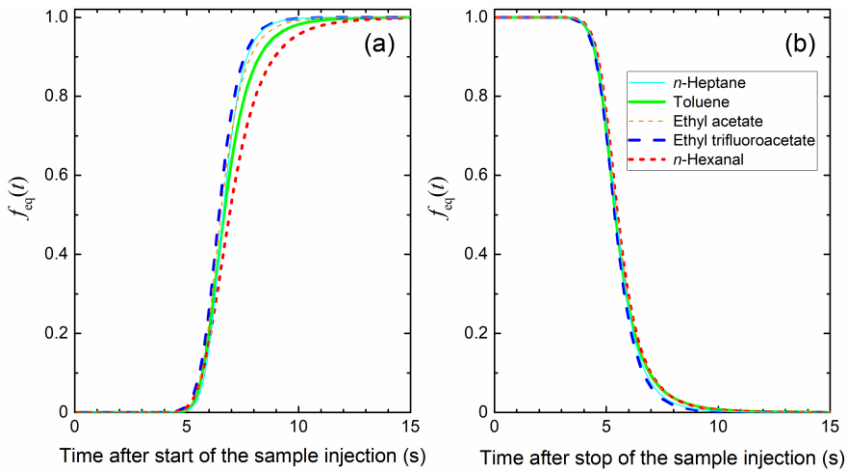

Figure 2. Parts of $f_{eq}(t)$ determined experimentally for each test compound.

$P_{\text{in}} f(t)$ and $P_{\text{c}}(t)$ in Eq. 6 can be replaced by $P_{\text{in}} f_{\text{eq}}(t)$ and $P_{\text{output}}(t)$, respectively, meaning that Eq. 6 can be rewritten as Eq. 16:

$$\frac{\mathrm{d}P_{\text{output}}(t)}{\mathrm{d}t} = \frac{F_G}{V_G}\frac{T}{T_0}P_{\text{in}}f_{\text{eq}}(t) - \frac{RT}{V_G}S_{\text{GL}}K_{\text{MO}} \times \left(HP_{\text{output}}(t) - C(t)\right) - \frac{F_G}{V_G}\frac{T}{T_0}P_{\text{output}}(t) \quad (16)$$

Because we simulated $x_{\text{obs}}(t)$ (= $P_{\text{obs}}(t)/P_{\text{in-obs}}$), substituting $x_{\text{obs}}(t) = \alpha_{\text{corr}} P_{\text{output}}(t)/P_{\text{in}}$ into Eq. 16 and rearranging gives Eq. 17:

$$\frac{\mathrm{d}x_{\text{obs}}(t)}{\mathrm{d}t} = \frac{F_G}{V_G}\frac{T}{T_0}\alpha_{\text{corr}}\, f_{\text{eq}}(t) - \frac{RT}{V_G}S_{\text{GL}}K_{\text{MO}} \times \left(Hx_{\text{obs}}(t) - \frac{\alpha_{\text{corr}}}{P_{\text{in}}}C(t)\right) - \frac{F_G}{V_G}\frac{T}{T_0}x_{\text{obs}}(t) \quad (17)$$

In each experimental run, the partial pressure of the test compound after passing through the contactor, $P_{\text{obs}}(t)$, was measured every 30 s for at least 10^3 s. Before and after each run to measure $P_{\text{obs}}(t)$, the partial pressure of the test compound when the gas mixture did not pass through the contactor, $P_{\text{in-obs}}$, was measured several times, and then $x_{\text{obs}}(t)$ was determined. A four-port PTFE valve (Figure 1, *k*) was used to select whether or not the gas mixture passed through the contactor. Substituting $y(t) = \alpha_{\text{corr}} C(t) / P_{\text{in}}$ and $y_{\text{diol}}(t) = \alpha_{\text{corr}} C_{\text{diol}}(t) / P_{\text{in}}$ into Eqs. 17 and 7a–d gives the following equations:

For all of the test compounds examined,

$$\frac{\mathrm{d}x_{\text{obs}}(t)}{\mathrm{d}t} = \frac{F_G}{V_G}\frac{T}{T_0}\alpha_{\text{corr}}\, f_{\text{eq}}(t) - \frac{RT}{V_G}S_{\text{GL}}K_{\text{MO}} \times \left(Hx_{\text{obs}}(t) - y(t)\right) - \frac{F_G}{V_G}\frac{T}{T_0}x_{\text{obs}}(t) \quad (18)$$

The following equations were solved together with Eq. 18 for each test compound:

$$\frac{\mathrm{d}y(t)}{\mathrm{d}t} = \frac{S_{\text{GL}}K_{\text{MO}}}{V_L} \times \left(Hx_{\text{obs}}(t) - y(t)\right) \quad \text{(for toluene or ethyl acetate)} \quad (19a)$$

$$\frac{dy(t)}{dt} = \frac{S_{GL}K_{MO}}{V_L} \times (Hx_{obs}(t) - y(t)) - k_h y(t) \quad \text{(for ethyl trifluoroacetate)} \qquad (19b)$$

$$\frac{dy(t)}{dt} = \frac{S_{GL}K_{MO}}{V_L} \times (Hx_{obs}(t) - y(t)) - k_f y(t) + k_b y_{diol}(t) \quad \text{(for } n\text{-hexanal)} \qquad (19c)$$

and $$\frac{dy_{diol}(t)}{dt} = k_f y(t) - k_b y_{diol}(t) \quad \text{(for } n\text{-hexanal)} \qquad (19d)$$

Eqs. 18 and 19 were used to determine values of H, k_h, k_f, k_b, or K_{hyd} (= k_f/k_b) for each test compound along with values of K_{MO} and α_{corr} by fitting the simulation results to the observed values. The boundary conditions were $x_{obs}(0) = y\ (0) = y_{diol}(0) = 0$. An increase of F_g by the initial injection of SG-a at 0–300 s, which was an increase of 4.17×10^{-5} dm^3 s^{-1}, was taken into consideration in the simulation.

The parameter fitting was carried out in three steps. In the first step, all of the time-profiles for each test compound at each aqueous-phase stirring speed and temperature, that is, 12 time-profiles for toluene and 24 time-profiles each for ethyl acetate, ethyl trifluoroacetate, and *n*-hexanal, were fitted assuming that the value of H obeyed the van't Hoff equation (Eq. 20) and that the values of k_h, k_f, and k_b obeyed the Arrhenius equation (Eq. 21):

$$H_i(T) = H_i^{298} \exp\left\{-\frac{\Delta H_{sol,\,i}}{R} \times \left(\frac{1}{T} - \frac{1}{298.15}\right)\right\} \qquad (20)$$

where $H_i(T)$ is the value of H or H^* at temperature T; H_i^{298} is the value at 298.15 K for H or H^* and is denoted as H^{298} or H^{*298}, respectively; $\Delta H_{sol,i}$ is the enthalpy of dissolution of the test compound or the apparent enthalpy change corresponding to the temperature dependence of H^* and is denoted as ΔH_{sol} or ΔH_{sol}^*, respectively.

$$k_i(T) = {k_i}^{298} \exp\left\{-\frac{\Delta E_{ai}}{R} \times \left(\frac{1}{T} - \frac{1}{298.15}\right)\right\} \quad (21)$$

where $k_i(T)$ is the value of k_h, k_f, or k_b at temperature T; ${k_i}^{298}$ is the value at 298.15 K for k_h, k_f, or k_b and is denoted as ${k_h}^{298}$, ${k_f}^{298}$, or ${k_b}^{298}$, respectively; ΔE_{ai} is the activation energy for hydrolysis of ethyl trifluoroacetate, hydration of *n*-hexanal, or dehydration of *n*-hexane-1,1-diol in the aqueous phase and is denoted as ΔE_{ah}, ΔE_{af}, or ΔE_{ab}, respectively. Table S4 lists the value initially set for each parameter in the first step of the simulation.

In the second step, the parameter fitting was performed individually for each time-profile. The initial values for each parameter were set as the values calculated from the thermodynamic parameters obtained in the first step. In the third step, parameter values were set as the values obtained in the second step, and the simulation was repeated with the initial value of H changed in increments of 0.1 M atm^{-1} in the range of ±1 M atm^{-1} for ethyl acetate and in increments of 0.01 M atm^{-1} in the range of ±0.1 M atm^{-1} for the other test compounds.

The parameter fitting was performed until a set of parameters that minimized the residual sum of squares (RSS) was obtained. The residual, R_{ij}, was defined by Eq. 22:

$$R_{ij} = (v_{ij} - u_{ij}) / \sigma_{ij} \quad (22)$$

where j was the jth point in time and i was the ith time series; v_{ij} was $x_{obs}(t)$ and u_{ij} was the corresponding value calculated in the simulation; and σ_{ij} was the weighting error. The values of σ_{ij} used for each test compound are listed in Table S4.

2.3.3 Perfect gas-phase mixing

As described in Section 2.3.1, the present analysis assumed perfect gas-phase mixing in the

385 contactor. The validity of this assumption was checked by estimating RTD based on the tanks-
386 in-series model (Levenspiel, 1999). In the tanks-in-series model, a flow is considered as a series
387 of tanks, that is, a series of perfect mixing flow units of a certain volume. Letting N be the
388 number of flow units, which corresponds to the gas phase flow in the contactor, its value is
389 given by Eq. 23 (Levenspiel, 1999):

390 $$N = \frac{(\Delta t_{\text{ave}})^2}{\Delta\sigma^2} \quad (23)$$

391 where Δt_{ave} and $\Delta\sigma^2$ are provided by Eqs. 24 and 25, respectively:

392 $$\Delta t_{\text{ave}} = t_{\text{ave, out}} - t_{\text{ave, in}} \quad (24)$$

393 $$\Delta\sigma^2 = {\sigma_{\text{out}}}^2 - {\sigma_{\text{in}}}^2 \quad (25)$$

394 where $t_{\text{ave,out}}$ and $t_{\text{ave,in}}$ are the average residence times of the output and input signals,
395 respectively; σ_{out} and σ_{in} are the variances of the residence time of the output and input signals,
396 respectively. The output signal and the input signal of the contactor correspond to $x_{\text{obs}}(t)$ and
397 $\alpha_{\text{corr}} f_{\text{eq}}(t)$, respectively, as indicated in Eq. 13; therefore, if perfect gas-phase mixing occurs in
398 the contactor, the value of N will be almost 1. In the next section, *n*-heptane was used as a tracer
399 to estimate N for the flow in the gas phase of the contactor.
400
401
402 **3. RESULTS AND DISCUSSION**
403 ***3.1 Evaluation of gas-phase mixing in the contactor***
404 *n*-Heptane was used as a tracer to examine the gas-phase mixing in the contactor and check the
405 validity of assuming perfect mixing. Figure 3 shows time-profiles of $x_{\text{obs}}(t)$ for *n*-heptane

(aqueous phase, deionized water stirred at 200, 300, or 400 rpm; gas phase was stirred at 300 rpm; temperature, 293.2 K). Figure 3 also shows $f_{eq}(t)$ for *n*-heptane, which is the same as the curve of *n*-heptane shown in Figure 2. As expected based on the small value of *H* for *n*-heptane (Sander, 2015), almost all of the test compound remained in the gas phase and passed through the contactor. This finding was supported by the fact that the time-profile of $x_{obs}(t)$ was almost identical regardless of the stirring speed of the aqueous phase.

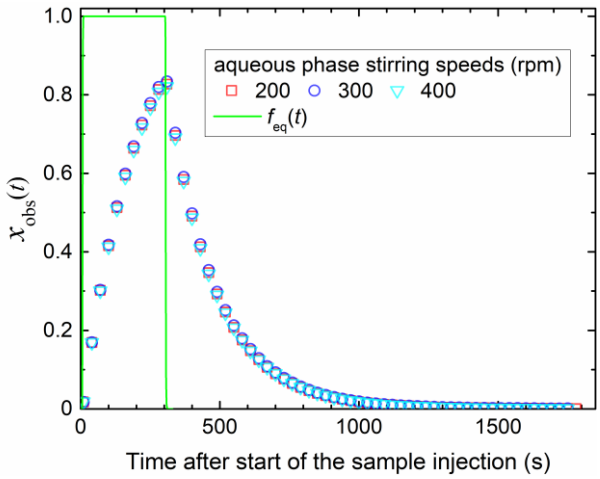

Figure 3. Time-profile of $x_{obs}(t)$ for *n*-heptane (aqueous phase, deionized water stirred at 200, 300, or 400 rpm; gas phase was stirred at 300 rpm; temperature, 293.2 K; P_{in}, 1.6×10^{-4} atm; flow rate of the *n*-heptane–N_2 mixture, 1.848×10^{-3} dm^3 s^{-1}). The green rectangle represents the time-profile of the input signal, $f_{eq}(t)$, of *n*-heptane, which is the same as the curve of *n*-heptane shown in Figure 2.

As described in Section 2.3.3, $t_{ave,out}$ and σ_{out}^2 can be calculated from the time-profile of $x_{obs}(t)$ according to Eqs. 26 and 27, respectively:

$$t_{ave,out} = \frac{\sum_{i=1}^{i=n} t_i \, x_{obs}(t_i)}{\sum_{i=1}^{i=n} x_{obs}(t_i)} \quad (26)$$

$$\sigma_{\text{out}}{}^2 = \frac{\sum_{i=1}^{i=n} t_i{}^2\, x_{\text{obs}}(t_i)}{\sum_{i=1}^{i=n} x_{\text{obs}}(t_i)} - t_{\text{ave,out}}{}^2 \quad (27)$$

where n is the number of data points in the time-profile. In a similar way, the values of $t_{\text{ave,in}}$ and $\sigma_{\text{in}}{}^2$ can be calculated from the time-profile of $f_{\text{eq}}(t)$ because α_{corr} does not influence the calculation. Table 1 lists these values, together with the values of Δt_{ave}, $\Delta\sigma^2$, and N, for the experimental runs conducted at the different stirring speeds. For each of the runs, N was close to 1, indicating that the assumption of perfect gas-phase mixing was appropriate for the present study.

Table 1. Values of t_{ave} and σ^2 for input and output signals and the resultant values of Δt_{ave}, $\Delta\sigma^2$, and N when n-heptane–N_2 mixture was passed through the contactor with different aqueous-phase stirring speeds.

$t_{\text{ave,in}}$ (s) [a]	$\sigma_{\text{in}}{}^2$ (s^2) [a]	Aqueous-phase stirring speed (rpm) [b]	$t_{\text{ave,out}}$ (s) [c]	$\sigma_{\text{out}}{}^2$ (s^2) [c]	Δt_{ave} (s) [d]	$\Delta\sigma^2$ (s^2) [d]	N [e]
156.16	7445.04	200	336.92	41726.36	180.76	34281.28	0.95
		300	338.60	42182.32	182.45	34737.28	0.96
		400	337.58	42255.32	181.42	34810.28	0.95

[a] $t_{\text{ave,in}}$ and σ_{in} are the average and the variance, respectively, of the residence time of the input signal.
[b] Gas-phase stirring speed was 300 rpm for all the runs.
[c] $t_{\text{ave,out}}$ and σ_{out} are the average and the variance, respectively, of the residence time of the output signal.
[d] Δt_{ave} and $\Delta\sigma^2$ are provided by Eqs. 24 and 25, respectively.
[e] N is the number of flow units in the tanks-in-series model; its value is given by Eq. 23.

3.2 Determination of H *values for toluene and ethyl acetate*

Figure 4 shows the time-profiles of $x_{\text{obs}}(t)$ for toluene and ethyl acetate (aqueous phase, deionized water stirred at 200, 300, or 400 rpm; gas phase was stirred at 300 rpm; temperature, 288.4 K). In each of the experimental runs, $x_{\text{obs}}(t)$ increased in the first 300 s and then rapidly decreased. Both the rate of increase and the rate of decrease of $x_{\text{obs}}(t)$ decreased with increasing aqueous stirring speed, suggesting that the rate of increase was decreased due to an increase in

the rate of dissolution of the compound, and that the rate of decrease was decreased due to an increase in the rate of volatilization of the dissolved compound, indicating that the mass-transfer rates of these compounds between the gas and aqueous phases increased with increasing aqueous stirring speed.

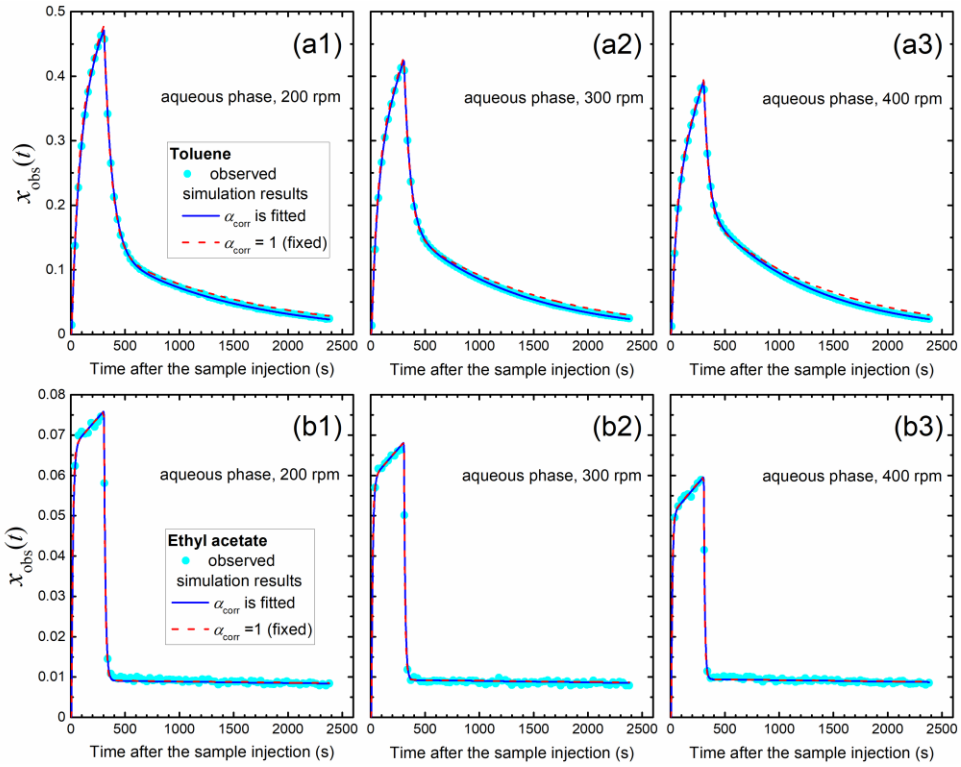

Figure 4. Time-profiles of $x_{obs}(t)$ for toluene (a) and ethyl acetate (b) (aqueous phase, deionized water stirred at 200 (a1, b1), 300 (a2, b2), or 400 (a3, b3) rpm; gas phase was stirred at 300 rpm; temperature, 288.4 K; P_{in}, 1.6×10^{-4} atm for toluene and 1.8×10^{-4} atm for ethyl acetate; flow rate of the compound–N_2 mixture, 1.837×10^{-3} dm^3 s^{-1}). Simulation results were obtained by using Eqs. 18 and 19a with α_{corr} as a fitting parameter (blue solid curve) or with α_{corr} bound to 1 (red dashed curve).

Next, simulations using Eqs. 18 and 19a were conducted to reproduce the time-profiles of $x_{obs}(t)$ with values of H and α_{corr} as common parameters and the value of K_{MO} as a parameter

dependent on the aqueous stirring speed. In the fitting procedure, the initial values of the parameters were set as described in Section 2.3.2. The blue curves in Figure 4 show the values of $x_{obs}(t)$ calculated in the simulation in which the RSS was minimized; the observed data were satisfactorily reproduced. In a similar way, we determined values of H, K_{MO}, and α_{corr} at different temperatures. The values determined are listed in Table S5 for toluene and in Table S6 for ethyl acetate. Values of α_{corr} were estimated as 0.920–0.927 for toluene and 0.862–0.887 for ethyl acetate at all of the temperatures examined. The red dashed curves in Figure 4 show the simulation results in which the value of α_{corr} was bound to 1. For toluene (Figure 4a1–3), these curves were slightly higher than the observed values after ca. 700 s, resulting in an RSS that was 22 times as large as that produced by the simulation using α_{corr} as a fitting parameter. For ethyl acetate (Figure 4b1–3), these curves appeared to reproduce well the observed data, but the RSS was about 1.5 times that produced by the simulation using α_{corr} as a fitting parameter.

Figure 5a shows van't Hoff plots of H for toluene and ethyl acetate; the values of H obeyed the van't Hoff equation. The values of H^{298} and ΔH_{sol} were determined by nonlinear regression of the data using Eq. 20 and a weighting factor of $(\text{error})^{-2}$, where the error is the error of the value of H at each temperature in the simulation. The determined values are listed in Table 2. Errors were at the 95% confidence level only for the weighted nonlinear regression of the data with Eq. 20. Table 2 also includes literature values of H^{298} and ΔH_{sol}. For toluene, because there are more than 70 studies containing relevant data (Sander, 2015), Table 2 includes only values from a review published in 2001 (Staudinger and Roberts, 2001) and from later studies (Bakierowska and Trzeszczyński, 2003; Bierwagen and Keller, 2001; Görgényi et al., 2002; Hiatt, 2013; Lee et al., 2013; Sieg et al., 2009) that reported both values of H^{298} and ΔH_{sol} without extrapolation from data obtained at high temperatures. For both toluene and ethyl

acetate, there is good agreement between the present results and the previously reported values of H^{298} and ΔH_{sol}.

Table 2. Values of H at 298.15 K and ΔH_{sol} for toluene and ethyl acetate in deionized water.

		This work [a]	Literature data
Toluene	H^{298} (M atm^{-1})	0.15 ± 0.02	0.15 [b, c], 0.16 [d], 0.17 [e, f, g], 0.21 [e]
	ΔH_{sol} (kJ mol^{-1})	−38.4 ± 7.4	−30 [f], −34 [d], −36 [b, c, e], −37 [g, h]
Ethyl acetate	H^{298} (M atm^{-1})	5.94 ± 0.27	5.9 [i], 6.0 [j], 6.3 [k]
	ΔH_{sol} (kJ mol^{-1})	−43.4 ± 2.7	−44 [i], −46 [k], −49 [j]

[a] Errors are at the 95% confidence level only for the weighted nonlinear regression of the data with Eq. 20. [b] Sieg et al. (2009). [c] Staudinger and Roberts (2001). [d] Görgényi et al. (2002). [e] Bakierowska and Trzeszczyński (2003). [f] Bierwagen and Keller (2001). [g] Lee et al. (2013). [h] Hiatt (2013). [i] Kieckbusch and King (1979). [j] Kutsuna et al. (2005). [k] Fenclová et al. (2014).

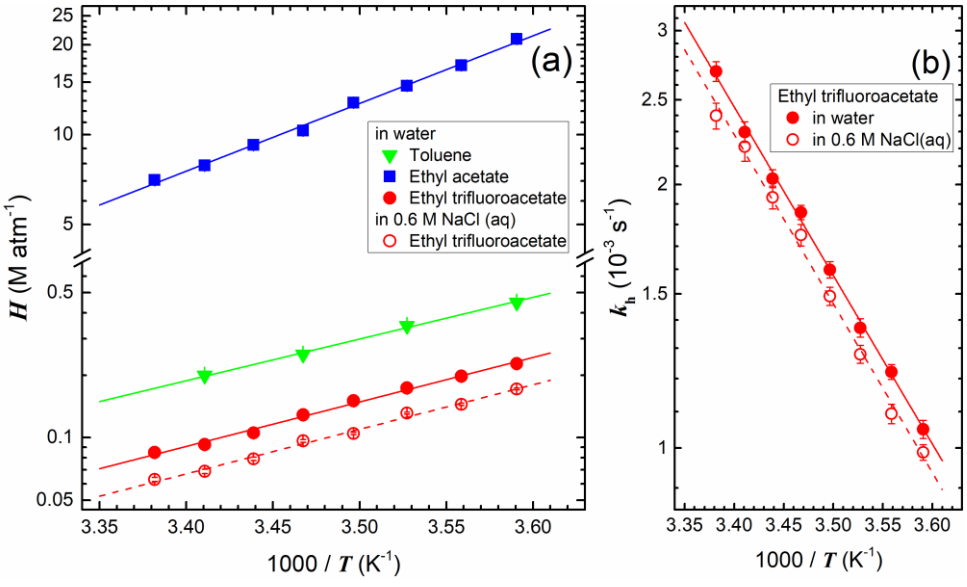

Figure 5. (a) van't Hoff plots of the values of H for toluene in deionized water (green triangles), ethyl acetate in deionized water (blue squares), and ethyl trifluoroacetate in deionized water (red closed circles) or 0.6 M aqueous NaCl (red open circles). Each line represents the weighted

499 nonlinear regression of the data using Eq. 20. (b) Arrhenius plots of k_h for ethyl trifluoroacetate
500 in deionized water (red closed circles) or 0.6 M aqueous NaCl (red open circles). Each line
501 represents the weighted nonlinear regression of the data using Eq. 21.
502
503 ***3.3 Determination of* H *and* k_h *values for ethyl trifluoroacetate***
504 Figure 6 shows time-profiles of $x_{obs}(t)$ for ethyl trifluoroacetate (aqueous phase, deionized
505 water or 0.6 M aqueous NaCl stirred at 200, 300, or 400 rpm; temperature, 288.4 K). Figure 6
506 also shows the results of simulations conducted with Eqs. 18 and 19b; the observed data were
507 satisfactorily reproduced. The maximum value of $x_{obs}(t)$ appeared at around 300 s and was
508 larger when the aqueous phase was 0.6 M aqueous NaCl than when it was deionized water,
509 suggesting that NaCl has a salting-out effect on ethyl trifluoroacetate in water.
510

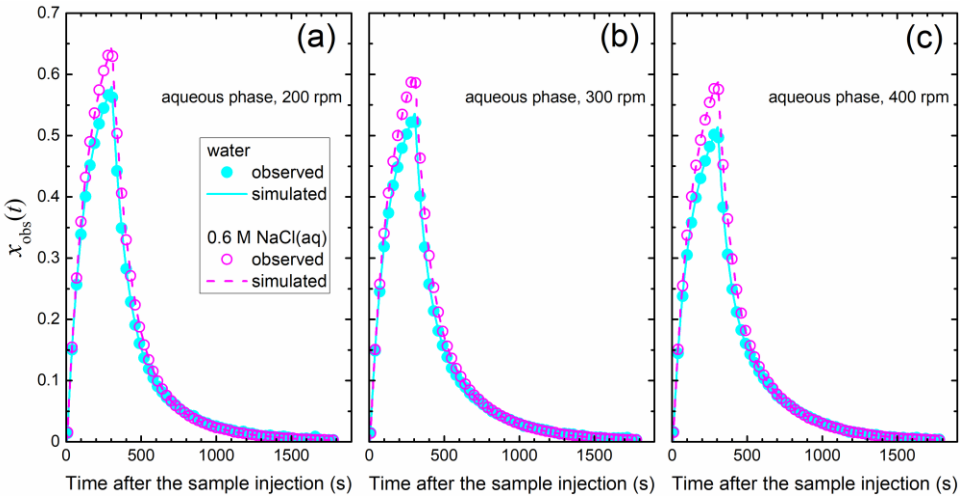

511

512 **Figure 6.** Time-profile of $x_{obs}(t)$ for ethyl trifluoroacetate (aqueous phase, deionized water or
513 0.6 M aqueous NaCl stirred at 200, 300, or 400 rpm; gas phase was stirred at 300 rpm;
514 temperature, 288.4 K; flow rate of ethyl trifluoroacetate–N_2 mixture, 1.837×10^{-3} dm^3 s^{-1}; P_{in},
515 1.5×10^{-4} atm). Simulation results were obtained by using Eqs. 18 and 19b.
516

Next, we determined values of H, k_h, K_{MO}, and α_{corr} for these two aqueous phases at a range of temperatures (278.5–295.7 K) (Tables S7 and S8). The values of α_{corr} ranged from 0.922 to 0.960. Figure 5a shows van't Hoff plots of H for ethyl trifluoroacetate in deionized water or 0.6 M aqueous NaCl. The values of H^{298} and ΔH_{sol} were determined by nonlinear regression of the data in a similar way as described for toluene and ethyl acetate. Figure 5b shows Arrhenius plots of the values of k_h for ethyl trifluoroacetate in deionized water or 0.6 M aqueous NaCl. The values of k_h^{298} and ΔE_{ah} were determined by nonlinear regression of the data with a weighting factor of $(\text{error})^{-2}$ using Eq. 21, where the error is the error of the value of k_h at each temperature.

Table 3 shows the values determined for H^{298}, ΔH_{sol}, k_h^{298}, and ΔE_{ah} as well as values from the published literature. For 0.6 M aqueous NaCl, to the authors' knowledge, there are no literature data available; however, the salting coefficient (k_s) for H was reported to be 0.74 kg mol^{-1} at 288.15 K by one of the present authors (Kutsuna et al., 2005). When converted to dm^3 mol^{-1}, the reported value becomes 0.71. Furthermore, taking errors into account for the linear fitting of the data with Eq. 28, the reported value becomes 0.71 ± 0.13. Here, the salting coefficient is defined using the Sechenov equation (Eq. 28):

$$\ln\left(\frac{H_0}{H_S}\right) = k_s m_S \qquad (28)$$

where H_0 and H_S are the Henry's law constants in deionized water and in an aqueous solution of salt S with ionic strength m_s (in M), respectively.

As shown in Table 3, our values of the thermodynamic parameters agree with those in the published literature. The values of k_h^{298} and ΔE_{ah} were deliberately determined with a smaller

error range than that of the reported values. The value of H^{298} for 0.6 M aqueous NaCl was smaller than that for deionized water, confirming the salting-out effect of NaCl on ethyl trifluoroacetate. In contrast, there was no difference in the value of ΔH_{sol} between the two solutions. The value of k_s was calculated as 0.51 ± 0.16 by using Eq. 28. This value agrees with the literature value (0.71 ± 0.13) after correcting the units, as described above. Furthermore, the salting effect on the hydrolysis rate was smaller than that on the solubility; the ratio of the value of k_h^{298} in 0.6 M aqueous NaCl to that in deionized water was 0.92 ± 0.04, whereas the corresponding ratio for H^{298} was 0.74 ± 0.07. The values of ΔE_a were within the error range for deionized water and 0.6 M aqueous NaCl.

Table 3. Values of H and k_h at 298.15 K and their temperature dependence for ethyl trifluoroacetate in deionized water or 0.6 M aqueous NaCl.

	Deionized water		0.6 M aqueous NaCl solutions
	This work [a]	Literature data [a, b]	This work [a]
H^{298} (M atm^{-1})	0.072 ± 0.004	0.09 ± 0.01	0.053 ± 0.004
ΔH_{sol} (kJ mol^{-1})	−41 ± 3	−41 ± 5	−41 ± 3
k_h^{298} (10^{-3} s^{-1})	3.01 ± 0.08	3.7 ± 1.1	2.77 ± 0.11
ΔE_{ah} (kJ mol^{-1})	37 ± 2	48 ± 16	36 ± 3

[a] Errors are at the 95% confidence level only for the weighted nonlinear regression of the data with Eq. 20 or 21.
[b] Kutsuna et al. (2005)

3.4 Determination of H *and* K_{hyd} *values for* n*-hexanal*

Figure 7 shows time-profiles of $x_{obs}(t)$ for *n*-hexanal (aqueous phase: deionized water, 0.6 M aqueous NaCl, or 0.2 M aqueous Na_2SO_4 stirred at 200, 300, or 400 rpm; temperature, 278.5 K). The mass-transfer rate between the gas and aqueous phases increased with increasing aqueous phase stirring speed. Figure 7 also shows the results of the simulations conducted using Eqs. 18, 19c, and 19d with H, k_f, k_b, and α_{corr} used as fitting parameters and K_{MO} used as

a fitting parameter depending on the aqueous stirring speed. Values of H, k_f, k_b, K_{MO}, and α_{corr} for each aqueous phase at different temperatures were also determined (Tables S9–S11). Values of K_{hyd} were calculated using Eq. 8 and are also listed in these tables. Values of α_{corr} were in the range of 0.894–0.961, except when deionized water was the aqueous phase and the temperature was 295.7 K (α_{corr} = 0.989).

To show how the values of H, k_f, and k_b for *n*-hexanal were determined in the simulation, Figure 7 also shows the time-profiles of ethyl acetate when deionized water at 278.5 K was used as the aqueous phase. The value of H^* at 278.5 K for *n*-hexanal (19 M atm^{-1}) was as large as that for ethyl acetate (21 M atm^{-1}); therefore, the values of $x_{obs}(t)$ for *n*-hexanal were close to those for ethyl acetate at ca. 2000 s. Until that time, however, the time-profiles of *n*-hexanal were different from those of ethyl acetate. The maximum value of $x_{obs}(t)$ at ca. 300 s for *n*-hexanal was clearly larger than that for ethyl acetate, suggesting that the value of H for *n*-hexanal was smaller than that for ethyl acetate. The values of $x_{obs}(t)$ for both ethyl acetate and *n*-hexanal decreased rapidly after 300 s. After 300 s, the values of $x_{obs}(t)$ for ethyl acetate remained almost constant, suggesting that the decrease of ethyl acetate in the outflow gas phase was compensated for by volatilization of the ethyl acetate dissolved in the aqueous phase. In contrast, the values of $x_{obs}(t)$ for *n*-hexanal continued to gradually decrease. Such a slow decay suggests the occurrence of slow, reversible aqueous reactions.

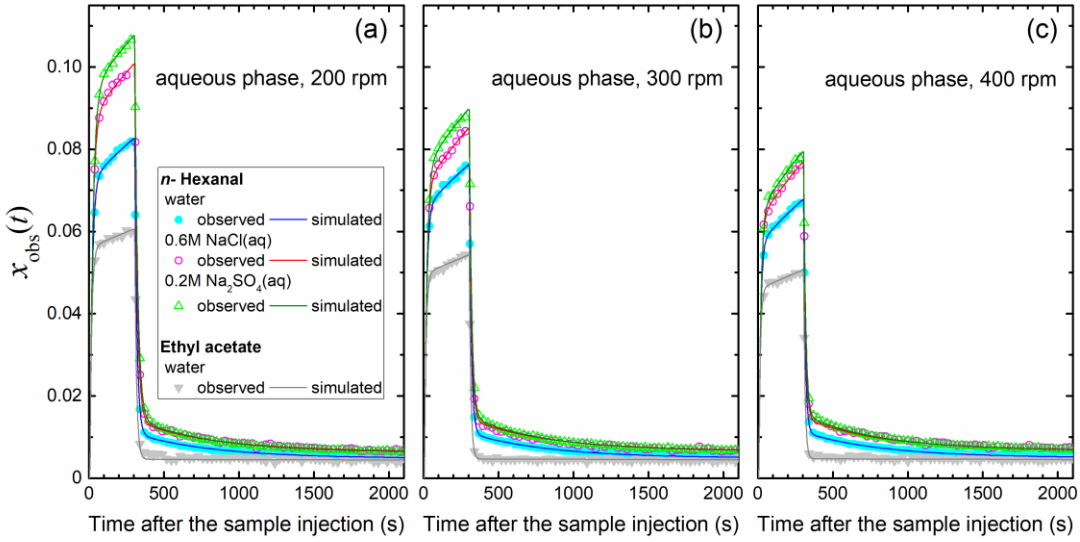

Figure 7. Time-profiles of $x_{obs}(t)$ for *n*-hexanal (aqueous phase: deionized water, 0.6 M aqueous NaCl, or 0.2 M aqueous Na_2SO_4 stirred at 200, 300, and 400 rpm; gas phase was stirred at 300 rpm; temperature, 278.5 K; P_{in}, 1.0×10^{-4} atm; flow rate of the compound–N_2 mixture, 1.822×10^{-3} dm^3 s^{-1}), and ethyl acetate (aqueous phase, deionized water; P_{in}, 1.8×10^{-4} atm; other parameters were as for *n*-hexanal). Solid lines show the simulation results obtained by using Eqs. 18, 19c, and 19d for *n*-hexanal and by using Eqs. 18 and 19a for ethyl acetate.

Thus, this difference in the time-profiles between ethyl acetate and *n*-hexanal is a result of the reversible hydration reaction of *n*-hexanal, and this difference, as well as the aforementioned behavior relating to the rates of dissolution and volatilization and the gas-to-water distribution of *n*-hexanal, allowed determination of the values of H, k_f, and k_b in the simulation.

Figure 8 shows the van't Hoff plots for H and H^* for the three aqueous phases. The values of H^* were calculated by using Eq. 4. The values of H^{298}, ΔH_{sol}, H^{*298}, and $\Delta H_{sol}{}^*$ were determined by nonlinear regression of the data with a weighting factor of $(\text{error})^{-2}$ by using Eq. 20, where the error is the error of the value of H or H^* at each temperature.

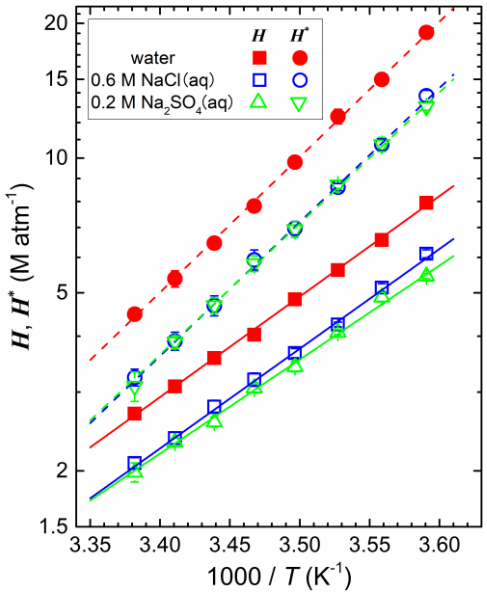

599

600 **Figure 8.** van't Hoff plots of the values of H and H^* for *n*-hexanal in deionized water, 0.6 M
601 aqueous NaCl, or 0.2 M aqueous Na_2SO_4. Solid and dashed lines represent the weighted
602 nonlinear fitting for the values of H and H^*, respectively, with Eq. 20.

603

604 Figure 9 shows the values of K_{hyd} on a logarithmic scale against inverse of temperature for each
605 solution; the values of K_{hyd} obeyed the following equation:

606 $$K_{hyd}(T) = {K_{hyd}}^{298} \exp\left\{-\frac{\Delta H_{hyd}}{R} \times \left(\frac{1}{T} - \frac{1}{298.15}\right)\right\} = \exp\left(-\frac{\Delta H_{hyd} - T\Delta S_{hyd}}{RT}\right) \quad (29)$$

607 where ${K_{hyd}}^{298}$ is the value of K_{hyd} at 298.15 K; and ΔH_{hyd} and ΔS_{hyd} are the enthalpy change and
608 entropy change, respectively, for the hydration. The right axis of each panel in Figure 9 shows
609 the values of k_f and k_b on a logarithmic scale for each solution. The values of k_f and k_b obeyed
610 the Arrhenius equation (Eq. 21). Nonlinear fitting of the data with a weighting factor of $(\text{error})^{-2}$
611 with Eq. 21 or 29, where the error is the error of each value of K_{hyd}, k_f, and k_b at each
612 temperature, provided values of ${K_{hyd}}^{298}$, ΔH_{hyd}, ΔS_{hyd}, ${k_f}^{298}$, ΔE_{af}, ${k_b}^{298}$, and ΔE_{ab}.

613

614 The values determined for the thermodynamic parameters are shown in Table 4. The value of

615 H^{298} was smaller in the aqueous salt solutions than in the deionized water, and the value in 0.6
616 M aqueous NaCl was comparable to that in 0.2 M aqueous Na_2SO_4. Thus, the salting-out effect
617 of NaCl and Na_2SO_4 on the solubility of *n*-hexanal was confirmed to depend on the ionic
618 strength, not the concentration, of the aqueous salt solution (Eq. 28). The salting coefficients,
619 k_s, of NaCl and Na_2SO_4 were calculated to be 0.43 ± 0.09 and 0.46 ± 0.09 M^{-1}, respectively.
620 These values were comparable to those of NaCl for ethyl trifluoroacetate (0.51 ± 0.16 M^{-1}). In
621 contrast, a salting effect on the value of ΔH_{sol} was not confirmed within the error range.
622

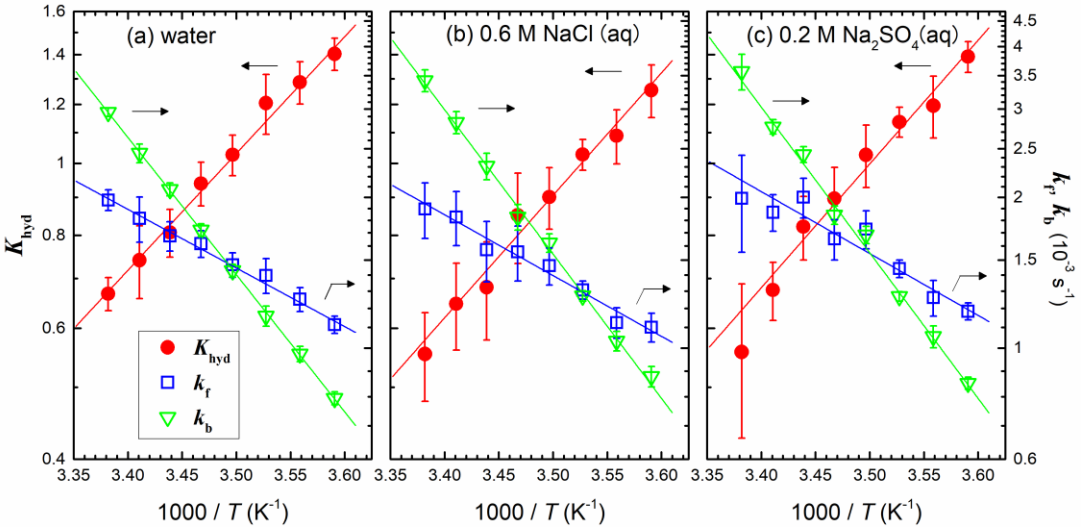

623

624 **Figure 9.** Semi-logarithmic plots of the values of K_{hyd} against 1000/T (red circles) and
625 Arrhenius plots of the values of k_f (blue squares) and k_b (green triangles) in deionized water (a),
626 0.6 M aqueous NaCl (b), or 0.2 M aqueous Na_2SO_4 (c). The solid line represents the weighted
627 nonlinear fitting for the values of K_{hyd} with Eq. 29. The dashed lines represent the weighted
628 nonlinear fitting for the values of k_f and k_b with Eq. 21.
629

630 **Table 4.** Values at 298.15 K for H, H^*, K_{hyd}, k_f, and k_b and their temperature dependence
631 determined for *n*-hexanal in deionized water, 0.6 M aqueous NaCl, or 0.2 M aqueous Na_2SO_4.

	Deionized water [a]	0.6 M NaCl (aq) [a]	0.2 M Na_2SO_4 (aq) [a]
H^{298} (M atm^{-1})	2.31 ± 0.06	1.78 ± 0.08	1.75 ± 0.08
ΔH_{sol} (kJ mol^{-1})	−43.0 ± 1.4	−42.7 ± 2.2	−40.2 ± 2.0
H^{*298} (M atm^{-1})	3.64 ± 0.10	2.63 ± 0.11	2.67 ± 0.10
ΔH_{sol}^* (kJ mol^{-1})	−57.9 ± 1.5	−57.3 ± 2.0	−56.1 ± 1.7
K_{hyd}^{298}	0.61 ± 0.03	0.52 ± 0.05	0.57 ± 0.06
ΔH_{hyd} (kJ mol^{-1})	−30.1 ± 2.3	−31.5 ± 4.4	−31.9 ± 4.6
ΔS_{hyd} (J mol^{-1} K^{-1})	−105 ± 8	−111 ± 15	−112 ± 16
k_f^{298} (10^{-3} s^{-1})	2.14 ± 0.08	2.10 ± 0.19	2.34 ± 0.30
ΔE_{af} (kJ mol^{-1})	22.4 ± 1.9	23.2 ± 4.3	23.7 ± 5.7
k_b^{298} (10^{-3} s^{-1})	3.52 ± 0.03	4.06 ± 0.23	4.12 ± 0.32
ΔE_{ab} (kJ mol^{-1})	52.5 ± 0.6	55.2 ± 3.0	55.7 ± 3.9

632 [a] Errors represent errors at the 95% confidence level only for the fitting by Eq. 20, 21, or 29.
633

634 The value of K_{hyd}^{298} in the aqueous salt solutions was smaller than that in deionized water, but
635 the difference was within the error range. The value of k_b^{298} was larger in the aqueous salt
636 solutions than in the deionized water. The value of ΔS_{hyd} has been suggested to represent the
637 entropy difference due to water molecules binding to *n*-hexanal during hydration (Buschmann
638 et al., 1982). Because the entropy difference between liquid water and ice is about 25 J mol^{-1}
639 K^{-1}, our value of ΔS_{hyd} of −105 J mol^{-1} K^{-1} shows that four water molecules are involved in
640 the hydration of *n*-hexanal, which is consistent with a previous report (Sham and Joens, 1995).
641

642 Furthermore, activation free energy ($\Delta G^‡$, in kJ mol^{-1}) and activation entropy ($\Delta S^‡$, in J mol^{-1}
643 K^{-1}) of the hydration reaction of *n*-hexanal was estimated. As shown in Supplementary material,
644 by applying absolute rate theory or transition state theory, $\Delta S^‡$ is calculated from the values of

645 k_f^{298} and ΔE_{af} (Table 4) to be −229 ± 6, −227 ± 15, and −224 ± 19 in deionized water, 0.6 M
646 aqueous NaCl, and 0.2 M aqueous Na_2SO_4, respectively (Table S12). Large ratio of
647 $(-T\Delta S^{\ddagger})/\Delta G^{\ddagger}$, which is calculated at 0.76–0.77, indicates that the hydration reaction of *n*-
648 hexanal is determined mainly by an entropic effect.
649
650 Table 5 shows experimentally determined literature values for the thermodynamic parameters
651 of *n*-hexanal and the method used for each determination as well as our data determined in the
652 present study. For the values of H or H^*, all the reported values in Table 5 are actually H^* values
653 because of the experimental methods that were used. The value of H^{*298} determined in the
654 present study was in good agreement with the statically determined value of 3.7 M atm^{-1}
655 (Jouquand et al., 2004) and was ca. 0.8 times the other values reported from direct measurement
656 using a static method (Buttery et al., 1969; Zhou and Mopper, 1990). In contrast, the value of
657 H^{*298} determined in the present study was 1.3 and 1.5 times the values determined by dynamic
658 absorption (Bruneel et al., 2016) and dynamic stripping (Karl et al., 2003), respectively. For
659 the absolute value of ΔH_{sol}^*, the value determined in the present study was larger by 4 or 8 kJ
660 mol^{-1} than the literature values determined by static methods (Jouquand et al., 2004; Zhou and
661 Mopper, 1990), and it was smaller by 5 or 18 kJ mol^{-1} than those determined by dynamic
662 methods (Bruneel et al., 2016; Karl et al., 2003). The reason for these differences is unclear.
663 These differences might be related to long time-constants used for the reversible hydration
664 reactions of *n*-hexanal. However, it is unlikely that long time-constants are able to fully explain
665 these differences, as shown in the next paragraph.
666
667 The time constants for the hydration equilibrium of *n*-hexanal are calculated from the values
668 of $(k_f + k_b)^{-1}$ to be 177–530 s at a temperature range of 278–298 K and increased with
669 decreasing temperature. Thus, for the static method by Zhou and Mopper (Zhou and Mopper,

1990), the partial pressure of *n*-hexanal was probably underestimated because it was measured in the gas mixture after purging the test solution in which the hydration equilibrium was not maintained, suggesting that $H^* < H_{stz}^*$, where H_{stz}^* is the effective Henry's law constant determined by their method. In contrast, for the dynamic stripping method (Karl et al., 2003), inequality 30 probably applied because the hydration equilibrium was not maintained in the test solution in the stripping cell.

$$\frac{F_s}{H^* RTV_{sl}} < \frac{|\Delta P_{ds}(t)|}{P_{ds}(t)} < \frac{F_s}{HRTV_{sl}} \quad (30)$$

where $P_{ds}(t)$ is partial pressure of *n*-hexanal measured at time t; $\Delta P_{ds}(t)$ is the change of $P_{ds}(t)$ per a second; F_s and V_{sl} are a gas flow rate and volume of the test solution, respectively, in the dynamic stripping experiment. Therefore, letting H_{ds}^* be the effective Henry's law constant determined by the dynamic stripping method, it is probable that $H < H_{ds}^* < H^*$ for determination using a single or two stripping cells (Karl et al., 2003). For the dynamic absorption method, the absorption experiment was reported to be stopped at the moment when the outlet concentration was equal for at least five minutes to the inlet concentration (Bruneel et al., 2016). It suggests that the hydration equilibrium was mostly maintained at 298 K but was not at 278 K; therefore, it is probable that $H < H_{da}^* < H^*$, where H_{da}^* is the effective Henry's law constant determined by the dynamic absorption method. Inequalities of $H^* < H_{stz}^*$, $H < H_{ds} < H^*$, and $H < H_{da} < H^*$ are qualitatively consistent with the difference between the values determined in the present study and those in the literature (Bruneel et al., 2016; Karl et al., 2003; Zhou and Mopper, 1990) (Table 5). However, this would mean that as the hydration process moves further from equilibrium with decreasing temperature, the absolute value of the dynamically determined ΔH_{sol}^* value would decrease, which is opposite to our present observations. Therefore, long time-constants for the reversible hydration reactions of *n*-hexanal still do not explain the

693 difference in the values determined by the different methods.

694

695 The value of K_{hyd}^{298} determined in the present study was between two reported values
696 (Buschmann et al., 1982; Sham and Joens, 1995). Taking into consideration the errors reported
697 in the literature, both values of K_{hyd}^{298} and ΔE_{hyd} agreed with those in the literature (Sham and
698 Joens, 1995). The values of k_f^{298} and k_b^{298} determined here were 0.60 and 0.83 times,
699 respectively, those reported in the literature (Buschmann et al., 1982). To the authors'
700 knowledge, this is the first report containing values of ΔE_{af} and ΔE_{ab}. As shown above, the
701 value of H and K_{hyd} determined in the present study agreed with some, but not all, of the
702 literature data. The reason for this is unclear; however, because the values of H and K_{hyd} in the
703 present study were determined simultaneously, the determined values are at least self-
704 consistent.

705 **Table 5.** Experimentally determined literature values of H, H^*, K_{hyd}, k_f, and k_b for *n*-hexanal
706 and deionized water, and the determined values in the present study.

H^{298} (M atm^{-1})	H^{*298} (M atm^{-1})	ΔH_{sol} (kJ mol^{-1})	$\Delta H_{sol}{}^{*}$ (kJ mol^{-1})	Method	Reference
	4.5			Static (direct measurement)	Buttery et al. (1969)
	4.8 [a]		−54 [a]	Static (direct measurement)	Zhou and Mopper (1990)
	3.7		−50 [b]	Static (phase ratio variation)	Jouquand et al. (2004)
	2.5 [c]		−63	Dynamic stripping method [d]	Karl et al. (2003)
	2.9		−76 [e]	Dynamic absorption method	Bruneel et al. (2016)
2.3	3.6	−43	−58	Rectangular pulse method	This work

$K_{hyd}{}^{298}$	ΔH_{hyd} (kJ mol^{-1})	$k_f{}^{298}$ (10^{-3} s^{-1})	$k_b{}^{298}$ (10^{-3} s^{-1})	Method	Reference
0.41 [f]				NMR	Buschmann et al. (1980)
0.83 [f]	−21	3.5	4.2	NMR, UV measurement	Buschmann et al. (1982)
0.49	−25.3			UV measurement	Sham and Joens (1995)
0.61	−29.7	2.1	3.5	Rectangular pulse method	This work

707 [a] Data from Table 1 by reference (Zhou and Mopper, 1990) were used to redo the regression analysis (Sander,
708 2015).
709 [b] Data from Tables 3 and 4 in reference (Jouquand et al., 2004) were used for the present authors to redo the
710 regression analysis after the partition coefficients were converted to units of M atm^{-1}.
711 [c] This value was calculated by the present authors from the data at 295 K (3.2 M atm^{-1}) and the temperature
712 dependence listed in Table 2 of reference (Karl et al., 2003).
713 [d] In reference (Karl et al., 2003), it was not specified whether single or two stripping cells were used to determine
714 the value of H for *n*-hexanal and its temperature dependence.
715 [e] Data from Table 1 in reference (Bruneel et al., 2016) were used for the present authors to redo the regression
716 analysis after the partition coefficients were converted to units of M atm^{-1}.
717 [f] References (Buschmann et al., 1980) and (Buschmann et al., 1982) are from the same research group. In reference
718 (Buschmann et al., 1982), the value of 0.41 was updated to 0.83.
719

720

721 ***3.5 Estimation of the liquid-film enhancement factor for mass transfer with aqueous***
722 ***reactions and mass-transfer limitation***

723 As described in Section 2.3.1, in the simulation, the equations assumed that the liquid-film
724 enhancement factor for mass transfer with aqueous reactions (E_L) was 1; in other words, the

aqueous reactions of ethyl trifluoroacetate and *n*-hexanal were assumed to proceed not in the liquid film but in the body of the liquid. We checked this assumption using the determined values of k_h, k_f, k_b, and K_{MO} and the Higbie penetration theory as follows.

The value of K_{MO} depends on the gas-film mass-transfer coefficient, k_{MG}, and the liquid-film mass-transfer coefficient, k_{ML}, as follows:

$$\frac{1}{K_{MO}} = \frac{HRT}{k_{MG}} + \frac{1}{k_{ML}} \quad (31)$$

According to the Higbie penetration theory, the gas–liquid interface consists of a variety of small liquid and gas elements, which are continuously brought to the surface from the bulk phase by the motion of the phases themselves (Biard et al., 2016). The values of k_{MG} and k_{ML} are given by Eqs. 32 and 33, respectively:

$$k_{MG} = \sqrt{\frac{4D_G}{\pi\tau_G}} \quad (32)$$

$$k_{ML} = \sqrt{\frac{4D_L}{\pi\tau_L}} \quad (33)$$

where D_G (in $dm^2\ s^{-1}$) is the gas-phase diffusion coefficient of the test compound in N_2; D_L (in $dm^2\ s^{-1}$) is the aqueous-phase diffusion coefficient of the test compound; τ_G (in s) and τ_L (in s) are the age of the small elements in the gas and liquid phases, respectively. Substituting Eqs. 32 and 33 into Eq. 31 gives Eq. 34:

$$\frac{1}{K_{MO}} = \frac{HRT}{\sqrt{\frac{4D_G}{\pi\tau_G}}} + \frac{1}{\sqrt{\frac{4D_L}{\pi\tau_L}}} \quad (34)$$

743 Eq. 34 can be rewritten as the following linear relationship (Biard et al., 2016):

744 $$\frac{\sqrt{\frac{4D_L}{\pi}}}{K_{MO}} = \sqrt{\tau_G} HRT \sqrt{\frac{D_L}{D_G}} + \sqrt{\tau_L} \quad (35)$$

745 As shown in the Supplementary material, the values of D_G and D_L were estimated according to
746 the equation of Fuller et al. (Eq. S10) (Fuller et al., 1966; Tang et al., 2014) and the correlation
747 of Hayduk and Laudie (Eq. S11) (Hayduk and Laudie, 1974), respectively. To calculate D_L,
748 the molar volume at the standard boiling point was substituted into Eq. S11 for toluene and
749 ethyl acetate (Hayduk and Laudie, 1974), and the molar volume at ambient temperature was
750 used for ethyl trifluoroacetate and *n*-hexanal. The values of D_G and D_L calculated for each
751 sample at each temperature are shown in Table S13.
752
753 Figure 10 shows the value of the left side of Eq. 35 plotted against the value of $HRT(D_L/D_G)^{0.5}$
754 for toluene, ethyl acetate, ethyl trifluoroacetate, and *n*-hexanal at different temperatures
755 (aqueous phase, deionized water stirred at 200, 300, or 400 rpm), and the figure clearly shows
756 the linear relationship described by Eq. 35. Furthermore, these plots suggest that the values of
757 τ_G and τ_L are insensitive to temperature under the experimental conditions examined. The
758 values of $\tau_G^{0.5}$ and $\tau_L^{0.5}$ can be determined as the slope and y-intercept, respectively, in each
759 panel. Table 6 shows the values of τ_G and τ_L. Errors are at the 95% confidence level only for
760 the linear regression of the data. The values of τ_G were expected to be constant because the gas-
761 phase stirring speed was kept constant, but it was found to have decreased by ca. 20% as the
762 aqueous-phase stirring speed increased from 200 to 400 rpm. This decrease was probably
763 induced via larger motion of aqueous surface waves with increasing stirring speed. The value
764 of τ_L decreased with increasing stirring speed and was roughly proportional to (stirring

765 speed)$^{-1.8}$.

766

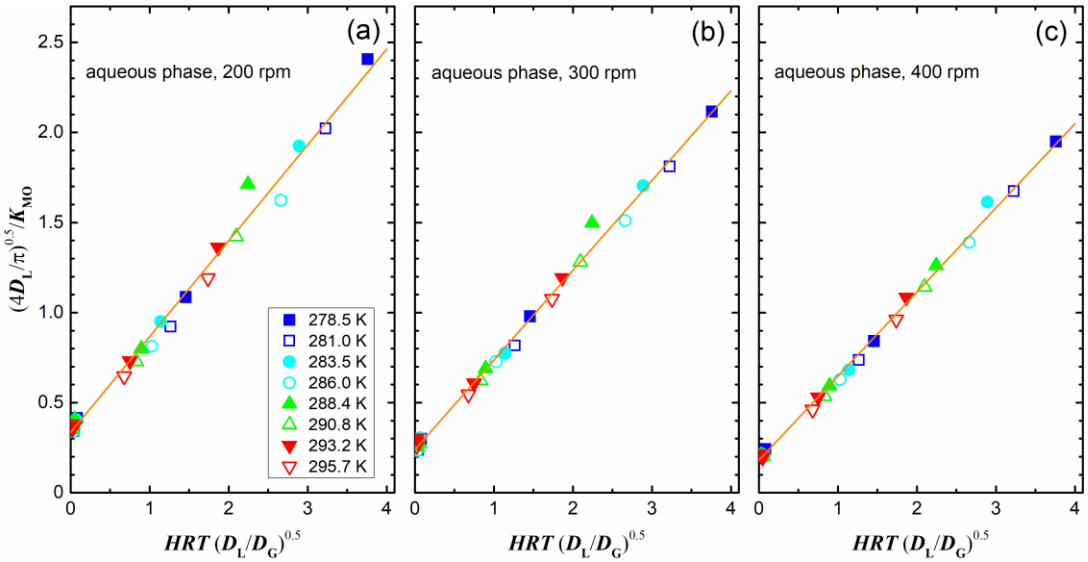

767

768 **Figure 10.** Plots of $(4D_L/\pi)^{0.5}/K_{MO}$ against $HRT(D_L/D_G)^{0.5}$ for toluene, ethyl acetate, ethyl
769 trifluoroacetate, and *n*-hexanal (aqueous phase, deionized water stirred at a speed of 200 (a),
770 300 (b), and 400 (c) rpm; gas phase was stirred at 300 rpm). Lines represent linear regressions
771 of the data with Eq. 35.

772

773 **Table 6.** Values of τ_G and τ_L at different aqueous-phase stirring speeds.

	Aqueous-phase stirring speed (rpm)		
	200	300	400
τ_G (s) [a]	0.283 ± 0.030	0.248 ± 0.020	0.218 ± 0.014
τ_L (s) [a]	0.112 ± 0.045	0.057 ± 0.030	0.033 ± 0.018

774 [a] Errors are at the 95% confidence level, with errors propagating only from those for the fitting with Eq. 35.
775

776 For aqueous reactions with a first-order reaction rate constant of k_1 (in s^{-1}), letting R_{bd} (in %)
777 be the ratio of the decrease of the test compound through reactions in the body of the aqueous
778 phase to that through reactions in the whole of the aqueous phase, the value of R_{bd} is estimated
779 using the value of τ_L as follows:

$$R_{\mathrm{bd}} > 100\exp(-k_1\tau_{\mathrm{L}}) \quad (36)$$

Inequality 36 can then be used to check the assumption of E_{L} = 1. The value of R_{bd} was estimated to be >99.9 from the values of k_{h}, k_{f}, and k_{b} for deionized water for all of the experimental runs for ethyl trifluoroacetate and *n*-hexanal. The assumption that the value of E_{L} is 1 is therefore self-consistent and is judged to be appropriate.

Finally, the values of k_{MG}, k_{ML}, and K_{MO} were calculated by using Eqs. 31–33. The percentage of resistance in the liquid phase (R_{L}, Eq. 37), which was a pertinent parameter to assess in which phase the mass transfer is mainly limited, and the relative error, which was calculated between the experimental value of K_{MO} and that calculated from Eq. 31, were also calculated as reported elsewhere (Biard et al., 2016).

$$R_{\mathrm{L}} = \left(1 + \frac{HRTk_{\mathrm{ML}}}{k_{\mathrm{MG}}}\right)^{-1} \quad (37)$$

These values are listed in Tables S14–S17. Table 7 shows the values at 278.5 and 293.2 K summarized from the supplementary tables.

Table 7. Mass-transfer coefficients, relative errors (RE) between the experimental and calculated values of K_{MO}, and percentage of resistance in the liquid phase (R_{L}).

Sample	Stirring speed (rpm)	10^4 K_{MO} MODEL[a] (dm s^{-1})	RE (%)	10^4 k_{ML} [b] (dm s^{-1})	10^2 k_{MG} [c] (dm s^{-1})	R_{L} (%)
at 278.5 K						
Toluene	200	6.45	9.6	7.28	5.79	88.6
	300	8.73	7.6	10.2	6.19	85.5
	400	11.1	11.1	13.5	6.60	82.7
Ethyl acetate	200	1.08	3.1	7.51	6.02	14.3
	300	1.19	0.18	10.5	6.43	11.3

	400	1.30	0.70	13.9	6.86	9.3
Ethyl trifluoroacetate	200	6.79	3.8	7.26	5.47	93.5
	300	9.33	6.5	10.2	5.84	91.7
	400	12.1	5.5	13.4	6.23	89.9
n-Hexanal	200	2.17	2.2	7.19	5.63	30.1
	300	2.49	1.4	10.1	6.01	24.7
	400	2.79	2.4	13.3	6.41	21.0
at 293.2 K						
Toluene	200	8.86	2.8	9.53	6.06	93.0
	300	12.2	7.0	13.4	6.47	91.0
	400	15.7	3.5	17.6	6.90	89.1
Ethyl acetate	200	2.48	2.6	9.84	6.29	25.2
	300	2.82	2.2	13.8	6.72	20.4
	400	3.13	3.1	18.2	7.17	17.2
Ethyl trifluoroacetate	200	9.17	1.8	9.51	5.72	96.4
	300	12.7	21.2	13.3	6.11	95.4
	400	16.6	7.9	17.6	6.52	94.3
n-Hexanal	200	4.30	0.18	9.42	5.89	45.7
	300	5.16	0.47	13.2	6.29	39.0
	400	5.94	0.17	17.4	6.71	34.1

[a] Values are overall liquid-side mass-transfer coefficients between N_2 gas and deionized water which are calculated from the calculated values of k_{MG} (Eq. 32) and k_{ML} (Eq. 33) by using Eq. 31.
[b] Values are liquid-film mass-transfer coefficients in deionized water which are calculated using Eq. 33.
[c] Values are gas-film mass transfer coefficients in N_2 gas which are calculated using Eq. 32.

As seen in Table 7, the overall liquid-side mass-transfer coefficients (K_{MO}) of the samples examined, particularly of *n*-hexanal and ethyl acetate, were correlated with the diffusion coefficients determined using the Higbie penetration theory. This correlation provides support for the certainty of the values of H and K_{hyd} determined for *n*-hexanal. Under the present experimental conditions, liquid-phase resistance was dominant for toluene and ethyl trifluoroacetate, whereas gas-phase resistance was dominant for *n*-hexanal and ethyl acetate.

4. CONCLUSION

Using our rectangular pulse method, we determined simultaneously the following values of H

812 and K_{hyd} for *n*-hexanal in deionized water at a temperature range of 278.5–295.7 K: $H = 2.31$
813 $\times \exp[5170 \times (1/T - 1/298.15)]$, $K_{hyd} = 0.61 \times \exp[3620 \times (1/T - 1/298.15)]$; thus, $H^* = 3.64 \times$
814 $[6960 \times (1/T - 1/298.15)]$. Rate constants for the hydration of *n*-hexanal and the dehydration
815 of its hydrate in deionized water were also determined: $k_f = 2.14 \times 10^{-3} \times \exp[-2690 \times (1/T -$
816 $1/298.15)]$ and $k_b = 3.52 \times 10^{-3} \times \exp[-6310 \times (1/T - 1/298.15)]$. Time constants for the
817 hydration equilibrium were 177–530 s at a temperature range of 278–298 K and increased with
818 decreasing temperature.
819
820 The determined values of H^* for *n*-hexanal agreed with literature data determined by static
821 methods but disagreed with literature data determined dynamically. The reason for this
822 disagreement was unclear. Salting effects on the value of H, but not on the value of K_{hyd}, were
823 confirmed for 0.6 M aqueous NaCl and 0.2 M aqueous Na_2SO_4. We also determined values of
824 H and hydrolysis rate constants for toluene, ethyl acetate, and ethyl trifluoroacetate, and found
825 values that agreed with the literature data. The overall liquid-side mass-transfer coefficients of
826 the samples examined were correlated with the diffusion coefficients using the Higbie
827 penetration theory.
828
829 Thus, our rectangular pulse method enables simultaneous determination of values of H and rate
830 constants for liquid-phase reactions of compounds such as aliphatic aldehydes or fluorinated
831 esters, the gas-to-water mass transfer of which involves relatively slow aqueous reactions.
832 Analysis of gas-to-solid mass transfer, which involves adsorption and reaction processes, is an
833 alternative application of this method. Indeed, our group is using this method to study the
834 influence of relative humidity on the adsorption and reaction processes of gaseous iodine
835 molecules flowing over clay minerals to provide data for estimating the dry deposition rates of
836 iodine molecules on the ground surface after accidental release into the atmosphere from

nuclear power plants.

FUNDING SOURCE

This work was supported by the Japan Society for the Promotion of Science [grant numbers JP23310019, JP18K11633].

REFERENCES

Atkinson, R., Tuazon, E.C., Aschmann, S.M., 1995. Products of the Gas-Phase Reactions of O_3 with Alkenes. Environmental Science and Technology 29, 1860-1866.

Bakierowska, A.-M., Trzeszczyński, J., 2003. Graphical method for the determination of water/gas partition coefficients of volatile organic compounds by a headspace gas chromatography technique. Fluid Phase Equilibria 213, 139-146.

Besley, L.M., Bottomley, G.A., 1974. Vapour pressure of toluence from 273.15 to 298.15 K. Journal of Chemical Thermodynamics 6, 577-580.

Biard, P.-F., Coudon, A., Couvert, A., Giraudet, S., 2016. A simple and timesaving method for the mass-transfer assessment of solvents used in physical absorption. Chemical Engineering Journal 290, 302-311.

Bierwagen, B.G., Keller, A.A., 2001. Measurement of Henry's law constant for methyl tert-butyl ether using solid-phase microextraction. Environmental Toxicology and Chemistry 20, 1625-1629.

Brilli, F., Hortnagl, L., Bamberger, I., Schnitzhofer, R., Ruuskanen, T.M., Hansel, A., Loreto, F., Wohlfahrt, G., 2012. Qualitative and quantitative characterization of volatile organic compound emissions from cut grass. Environmental Science and Technology 46, 3859-3865.

862 Bruneel, J., Walgraeve, C., Van Huffel, K., Van Langenhove, H., 2016. Determination of the
863 gas-to-liquid partitioning coefficients using a new dynamic absorption method (DynAb
864 method). Chemical Engineering Journal 283, 544-552.
865 Buschmann, H.-J., Dutkiewicz, E., Knoche, W., 1982. The Reversible Hydration of Carbonyl
866 Compounds in Aqueous Solution Part II: The Kinetics of the Keto/Gem-diol Transition.
867 Berichte der Bunsengesellschaft fiir Physikalische Chemie 86, 129-134.
868 Buschmann, H.-J., Füldner, H.-H., Knoche, W., 1980. The Reversible Hydration of Carbonyl
869 Compounds in Aqueous Solution. Part I, The Keto/Gem-diol Equilibrium. Berichte der
870 Bunsengesellschaft fiir Physikalische Chemie 84, 41-44.
871 Buttery, R.G., Ling, L., Guadagni, D.G., 1969. Food volatiles. Volatilities of aldehydes, ketones,
872 and esters in dilute water solution. Journal of Agricultural and Food Chemistry 17, 385-389.
873 Carruth, G.F., Kobayashi, R., 1973. Vapor pressure of normal paraffins ethane through n-
874 decane from their triple points to about 10 mm mercury. Journal of Chemical and Engineering
875 Data 18, 115-126.
876 Covarrubias-Cervantes, M., Mokbel, I., Champion, D., Jose, J., Voilley, A., 2004. Saturated
877 vapour pressure of aroma compounds at various temperatures. Food Chemistry 85, 221-229.
878 Ervens, B., Kreidenweis, S.M., 2007. SOA formation by biogenic and carbonyl compounds:
879 data evaluation and application. Environmental Science and Technology 41, 3904-3910.
880 Fenclová, D., Blahut, A., Vrbka, P., Dohnal, V., Böhme, A., 2014. Temperature dependence of
881 limiting activity coefficients, Henry's law constants, and related infinite dilution properties of
882 C4–C6 isomeric n-alkyl ethanoates/ethyl n-alkanoates in water. Measurement, critical
883 compilation, correlation, and recommended data. Fluid Phase Equilibria 375, 347-359.
884 Fuller, E.N., Schettler, P.D., Giddings, J.C., 1966. New method for prediction of binary gas-
885 phase diffusion coefficients. Industrial and Engineering Chemistry 58, 18-27.
886 Görgényi, M., Dewulf, J., Langenhove, H.V., 2002. Temperature dependence of Henry's law

887 constant in an extended temperature range. Chemosphere 48, 757-762.
888 Grosjean, E., Grosjean, D., Seinfeld, J.H., 1996. Atmospheric Chemistry of 1-Octene, 1-
889 Decene, and Cyclohexene: Gas-Phase Carbonyl and Peroxyacyl Nitrate Products.
890 Environmental Science and Technology 30, 1038-1047.
891 Hayduk, W., Laudie, H., 1974. Prediction of diffusion coefficients for nonelectrolytes in dilute
892 aqueous solutions. AlChE Journal 20, 611-615.
893 Hiatt, M.H., 2013. Determination of Henry's Law Constants Using Internal Standards with
894 Benchmark Values. Journal of Chemical and Engineering Data 58, 902-908.
895 Huang, Z., Jiang, H., Li, L., Wang, H., Qiu, T., 2015. Density, viscosity, and saturated vapor
896 pressure of ethyl trifluoroacetate. Journal of Chemical Thermodynamics 86, 75-79.
897 Jouquand, C., Ducruet, V., Giampaoli, P., 2004. Partition coefficients of aroma compounds in
898 polysaccharide solutions by the phase ratio variation method. Food Chemistry 85, 467-474.
899 Karl, T., Yeretzian, C., Jordan, A., Lindinger, W., 2003. Dynamic measurements of partition
900 coefficients using proton-transfer-reaction mass spectrometry (PTR–MS). International
901 Journal of Mass Spectrometry 223-224, 383-395.
902 Kieckbusch, T.G., King, C.J., 1979. An Improved Method of Determining Vapor-Liquid
903 Equilibria for Dilute Organics in Aqueous Solution. Journal of Chromatographic Science 17,
904 273-276.
905 Kutsuna, S., 2018. Rate constants and C–C bond scission ratios for hydrolysis of 2,2,3-
906 trifluoro-3-(trifluoromethyl)oxirane determined by means of a closed-circulation reactor.
907 Journal of Fluorine Chemistry 211, 109-118.
908 Kutsuna, S., Chen, L., Abe, T., Mizukado, J., Uchimaru, T., Tokuhashi, K., Sekiya, A., 2005.
909 Henry's law constants of 2,2,2-trifluoroethyl formate, ethyl trifluoroacetate, and non-
910 fluorinated analogous esters. Atmospheric Environment 39, 5884-5892.
911 Lee, S.-H., Mukherjee, S., Brewer, B., Ryan, R., Yu, H., Gangoda, M., 2013. A Laboratory

912 Experiment To Measure Henry's Law Constants of Volatile Organic Compounds with a Bubble
913 Column and a Gas Chromatography Flame Ionization Detector (GC-FID). Journal of Chemical
914 Education 90, 495-499.
915 Levenspiel, O., 1999. Chemical reaction engineering, 3rd ed. John Wiley & Sons, NJ.
916 Lewis, W.K., Whitman, W.G., 1924. Principles of Gas Absorption. Industrial and Engineering
917 Chemistry 16, 1215-1220.
918 NIST Standard Reference Database Number 69. National Institute of Standards and
919 Technology, Gaithersburg MD, 20899.
920 Polák, J., Mertl, I., 1965. Saturated vapour pressure of methyl acetate, ethyl acetate, n-propyl
921 acetate, methyl propionate, and ethyl propionate. Collection of Czechoslovak Chemical
922 Communications 30, 3526-3528.
923 Sander, R., 2015. Compilation of Henry's law constants (version 4.0) for water as solvent.
924 Atmospheric Chemistry and Physics 15, 4399-4981.
925 Sham, Y.Y., Joens, J.A., 1995. Temperature dependent near UV molar absorptivities of several
926 small aldehydes in aqueous solution. Spectrochim Acta, Part A 51, 247-251.
927 Sieg, K., Starokozhev, E., Schmidt, M.U., Püttmann, W., 2009. Inverse temperature
928 dependence of Henry's law coefficients for volatile organic compounds in supercooled water.
929 Chemosphere 77, 8-14.
930 Staudinger, J., Roberts, P.V., 2001. A critical compilation of Henry's law constant temperature
931 dependence relations for organic compounds in dilute aqueous solutions. Chemosphere 44,
932 561-576.
933 Tang, M.J., Cox, R.A., Kalberer, M., 2014. Compilation and evaluation of gas phase diffusion
934 coefficients of reactive trace gases in the atmosphere: volume 1. Inorganic compounds.
935 Atmospheric Chemistry and Physics 14, 9233-9247.
936 Tang, Y., Zhu, L., 2004. Wavelength-Dependent Photolysis of *n*-Hexanal and *n*-Heptanal in the

280−330-nm Region. Journal of Physical Chemistry A 108, 8307-8316.

Winer, A.M., Arey, J., Atkinson, R., Aschmann, S.M., Long, W.D., Morrison, C.L., Olszyk, D.M., 1992. Emission rates of organics from vegetation in California's Central Valley. Atmospheric Environment 26, 2647-2659.

Zhou, S., Gonzalez, L., Leithead, A., Finewax, Z., Thalman, R., Vlasenko, A., Vagle, S., Miller, L.A., Li, S.M., Bureekul, S., Furutani, H., Uematsu, M., Volkamer, R., Abbatt, J., 2014. Formation of gas-phase carbonyls from heterogeneous oxidation of polyunsaturated fatty acids at the air–water interface and of the sea surface microlayer. Atmospheric Chemistry and Physics 14, 1371-1384.

Zhou, X., Mopper, K., 1990. Apparent partition coefficients of 15 carbonyl compounds between air and seawater and between air and freshwater; implications for air-sea exchange. Environmental Science and Technology 24, 1864-1869.

Glossary

$C(t)$: concentration of the test compound in the body of the liquid at time t (mol dm^{-3} or M)

$C_{diol}(t)$: concentration of hydrated aldehyde (geminal diol) in the body of the liquid at time t (M)

D_G (D_L): diffusion coefficient at infinite dilution of a solute in N_2 gas (in aqueous phase) (dm^2 s^{-1})

$E_c(t)$: residence time distribution (RTD) of the gas mixture passing through the gas–liquid contactor (dimensionless)

$E_{inlet}(t)$ ($E_{outlet}(t)$): RTD of the gas mixture passing through the inlet (outlet) region (dimensionless)

E_L: liquid-film enhancement factor for mass transfer with aqueous reactions (dimensionless)

ΔE_{ah}: activation energy for hydrolysis (kJ mol^{-1})

ΔE_{af}: activation energy for hydration of aldehydes (kJ mol^{-1})

ΔE_{ab}: activation energy for dehydration of hydrated aldehydes (geminal diols) (kJ mol^{-1})

F_g: total flow rate of the gas mixture passing through the gas–liquid contactor (dm^3 s^{-1})

F_s: gas flow rates in the dynamic stripping method (dm^3 s^{-1})

F_1 (F_2): N_2 gas flow rates controlled by mass-flow controller 1 (2) (dm^3 s^{-1})

$f(t)$: normalized time profile of the partial pressure of the rectangular input pulse (dimensionless)

$f_{eq}(t)$: normalized time profile for convolution of RTD of the inlet and outlet regions with the rectangular input pulse (dimensionless)

$\Delta G^{\ddagger}$: activation free energy for hydration of aldehydes (kJ mol^{-1})

H: Henry's law constant (M atm^{-1})

H^*: effective Henry's law constant (M atm^{-1})

H_{da}^*: effective Henry's law constant determined by the dynamic absorption method (M atm^{-1})

975 H_{ds}^{*}: effective Henry's law constant determined by the dynamic stripping method (M atm^{-1})

976 H_{stz}^{*}: effective Henry's law constant determined by the direct measurement in the static method
977 by Zhou and Mopper (Zhou and Mopper, 1990) (M atm^{-1})

978 ΔH_{hyd}: enthalpy change of hydration of aldehydes (kJ mol^{-1})

979 ΔH_{sol}: enthalpy of dissolution (kJ mol^{-1})

980 ΔH_{sol}^{*}: apparent enthalpy change corresponding to the temperature dependence of H^{*} (kJ
981 mol^{-1})

982 k_1: rate constant for first-order reactions (s^{-1})

983 k_b: rate constant for dehydration of geminal diol (s^{-1})

984 k_f: rate constant for hydration of aldehyde (s^{-1})

985 k_h: rate constant for hydrolysis (s^{-1})

986 K_{hyd}: hydration equilibrium constant (dimensionless)

987 K_{MO}: overall liquid-side mass-transfer coefficient from gas to liquid (dm s^{-1})

988 k_{MG}: gas-film mass-transfer coefficient (dm s^{-1})

989 k_{ML}: liquid-film mass-transfer coefficient (dm s^{-1})

990 k_s: salting coefficient (M^{-1})

991 N: number of flow units in the tanks-in-series model (dimensionless)

992 P_{in}: partial pressure of the test compound in the rectangular input pulse (atm)

993 $P_{in\text{-}obs}$: partial pressure measured at the GC-FID of the test compound in the rectangular input
994 pulse (atm)

995 $P_c(t)$: partial pressure of the test compound at time t in the gas–liquid contactor (atm)

996 $P_{ds}(t)$: partial pressure measured at time t while bubbles arise through the test solution in the
997 stripping cell in the dynamic stripping method (atm)

998 $\Delta P_{ds}(t)$: change of $P_{ds}(t)$ per a second (atm s^{-1})

999 $P_{obs}(t)$: partial pressure measured at the GC-FID at time t of the test compound in the gas

mixture leaving the gas–liquid contactor (atm)

$P_{output}(t)$: partial pressure measured at the GC-FID at time t with no measurement error of the test compound in the gas mixture leaving the gas–liquid contactor (atm)

R: gas constant (0.0821 atm dm^3 mol^{-1} K^{-1}, or 8.314 J mol^{-1} K^{-1})

R_{bd}: ratio of the decrease of the test compound through reactions in the body of the aqueous phase to that through reactions in the whole of the aqueous phase (%)

RE: relative error between a theoretical and an experimental value (%)

R_L: relative mass-transfer resistance in the liquid phase (%)

RSS: residual sum of squares

RTD: residence time distribution

S_{GL}: gas–liquid interface area in the gas–liquid contactor (dm^2)

ΔS_{hyd}: entropy change for hydration of aldehydes (J mol^{-1} K^{-1})

$\Delta S^{\ddagger}$: activation entropy for hydration of aldehydes (J mol^{-1} K^{-1})

T: temperature of the gas–liquid contactor (K)

T_0: 298.15 K

t: time after sample injection (s)

$t_{ave,in}$ ($t_{ave,out}$): average residence time of the input (output) signal (s)

Δt_{ave}: $\Delta t_{ave} = t_{ave,out} - t_{ave,in}$ (s)

V_G (V_L): gas-phase volume (aqueous-phase volume) in the gas–liquid contactor (dm^3)

V_{sl}: volume of the test solution in the dynamic stripping method (dm^3)

$x_{obs}(t)$: residence ratio measured at the GC-FID at time t of the test compound in the gas mixture leaving the gas–liquid contactor, which ratio is defined as $x_{obs}(t) = P_{obs}(t)/P_{in\text{-}obs} = \alpha_{corr} \times P_{output}(t)/P_{in}$ (dimensionless)

$y(t)$: concentration of the test compound in the body of the liquid at time t multiplied by α_{corr}/P_{in}, that is, $y(t) = \alpha_{corr}\, C(t) / P_{in}$ (M atm^{-1})

1025 $y_{diol}(t)$: concentration of hydrated aldehyde (geminal diol) in the body of the liquid at time t

1026 multiplied by α_{corr}/P_{in}, that is, $y_{diol}(t) = \alpha_{corr}\, C_{diol}(t) / P_{in}$ (M atm^{-1})

1027 *Greek letters*

1028 α_{corr}: potential calibration errors for $x_{obs}(t)$, and is defined by $\alpha_{corr} = x_{obs}(t) / (P_{output}(t)/P_{in})$

1029 (dimensionless)

1030 σ_{in} (σ_{out}): valiance of the residence time of the input (output) signal (s^2)

1031 $\Delta\sigma^2$: $\Delta\sigma^2 = \sigma_{out}^2 - \sigma_{in}^2$

1032 τ_{dl} (τ_{da}): time constant of gas-to-water transfer in dynamic stripping method with a single cell

1033 (dynamic stripping method with double cells and dynamic absorption method) (s)

1034 τ_G (τ_L): contact time of a gas element (liquid element) at the gas–liquid interface in the Higbie

1035 penetration theory (s)

1036 *Superscript*

1037 ^{298}: values at 298.15 K

1038

Supplementary material

Henry's Law Constants and Hydration Equilibrium Constants of *n*-Hexanal and Their Temperature Dependence as Determined by the Rectangular Pulse Method

Shuzo Kutsuna*, Naoki Kaneyasu

National Institute of Advanced Industrial Science and Technology (AIST),

16-1 Onogawa, Tsukuba, Ibaraki 305-8569, JAPAN

Corresponding author*: s-kutsuna@aist.go.jp

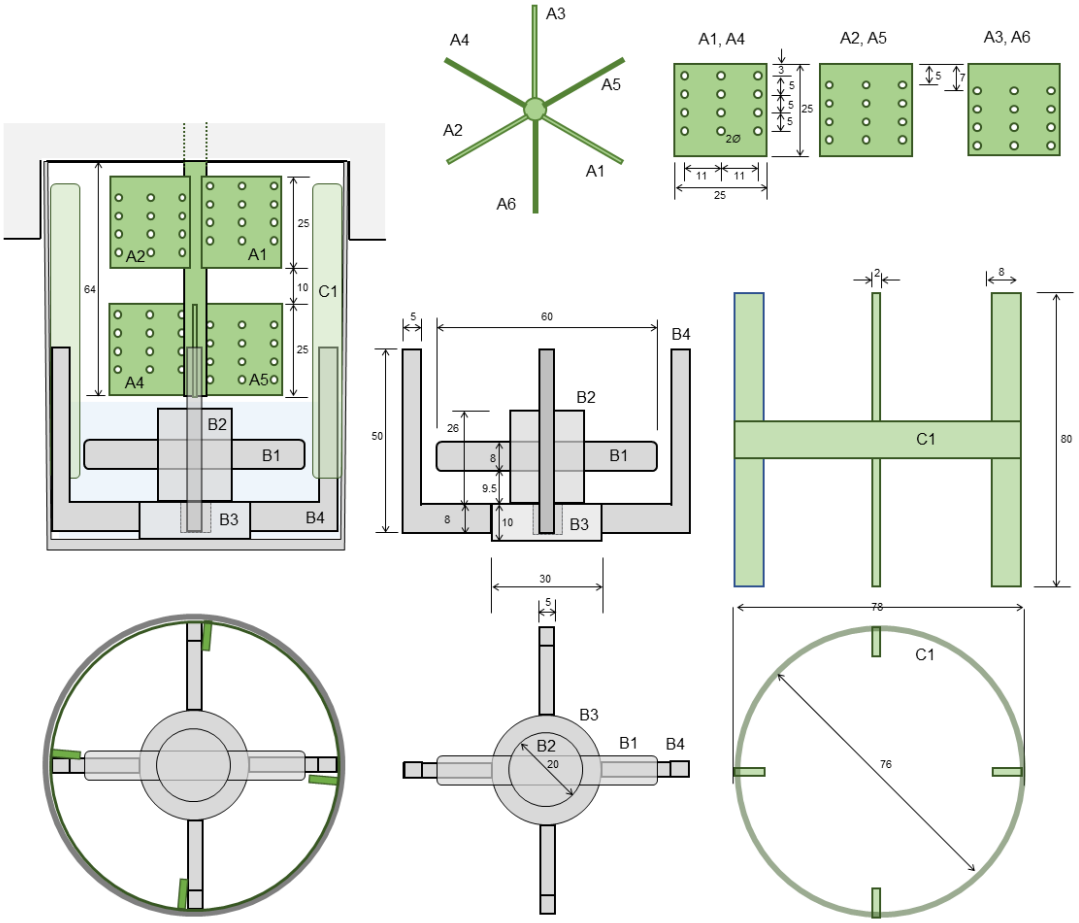

1049

1050 **Figure S1.** Schematic of the double-mixing gas–liquid contactor, and details of (A1–A6) six-
1051 blade turbine with 12 holes in each blade; (B1−B4) cylindrical PTFE magnetic stirring bar (B1)
1052 with a PTFE support (B2, B3) and four PTFE baffles (B4); (C1) four PTFE-coated stainless-
1053 steel baffles. Number represents length of each part in unit of mm.

1054

Table S1. Experimental conditions used for preparing SG-a and SG-b, and the concentration of the test compound in each gas.

	SG-a				SG-b
	T_s [a] (K)	F_1 [b] (10^{-3} dm^3 s^{-1})	F_2 [b] (10^{-3} dm^3 s^{-1})	concentration (ppmv)	concentration (ppmv)
n-Heptane	288.2	0.0767	0.291	7260	160
Toluene	288.2	0.0767	0.153	7321	161 – 162
Ethyl acetate	288.2	0.0767	0.613	8341	184 – 186
Ethyl trifluoroacetate	288.2	0.0307	0.613	6813	150 – 152
n-Hexanal	295.2	0.0767	0.153	4508	100 – 102

[a] T_s is the temperature of the aluminum block of the electronic dry bath (Figure 1, *b*).

[b] F_1 and F_2 are the N_2 gas flow rates controlled by mass-flow controllers 1 and 2 (Figure 1, MFC1 and MFC2), respectively.

Table S2. Experimental conditions for GC analysis of each sample.

	n-Heptane	Toluene	Ethyl acetate	Ethyl trifluoroacetate	*n*-Hexanal
column temperature (°C)	90	80	80	65	75
injection temperature (°C)	110	110	110	110	110
detector temperature (°C)	250	250	250	250	230
carrier gas	N_2	N_2	N_2	N_2	N_2
carrier gas pressure (kPa)	37.5	37.5	37.5	37.5	37.5
split ratio [a]	1:10	1:10	1:10	1:10	1:10

[a] The split ratio was constant through the experiment for continuous analysis of the sample every 30 s.

Independence of $E_c(t)$ on input signal (Section 2.3.2)

As described in Section 2.3.2, for all the test compounds in the present study, $E_c(t)$ does not change if the input signal is changed. This fact is demonstrated as follows.

For toluene and ethyl acetate, taking Laplace transform of Eqs. 6 and 7a, together with $P_c(0) = C(0) = 0$, yields Eqs. S1 and S2.

$$\lambda\overline{P_c(t)} = \frac{F_G}{V_G}\frac{T}{T_0}P_{in}\overline{f(t)} - \left(\frac{RTS_{GL}K_{MO}H}{V_G} + \frac{F_G}{V_G}\frac{T}{T_0}\right)\overline{P_c(t)} + \frac{RTS_{GL}K_{MO}}{V_G}\overline{C(t)} \quad \text{(S1)}$$

$$\lambda\overline{C(t)} = \frac{S_{GL}K_{MO}H}{V_L}\overline{P_c(t)} - \frac{S_{GL}K_{MO}}{V_L}\overline{C(t)} \quad \text{(S2)}$$

where $\overline{g(t)}$ is Laplace transform of $g(t)$: $\overline{g(t)} = \int_0^\infty g(t)\exp(-\lambda t)\,dt$. Rearranging Eqs. S1 and S2, $\overline{P_c(t)}$ is represented by Eq. S3.

$$\overline{P_c(t)} = P_{in}\overline{f(t)} \times \frac{\frac{F_G\,T}{V_G T_0}}{\lambda + \frac{HRTS_{GL}K_{MO}}{V_G} + \frac{F_G\,T}{V_G T_0} - \frac{\frac{HRTS_{GL}{}^2K_{MO}{}^2}{V_L V_G}}{\lambda + \frac{S_{GL}K_{MO}}{V_L}}} \quad \text{(S3)}$$

Eq. S3 shows that $\overline{E_c(t)}$ is given as follows:

$$\overline{E_c(t)} = \frac{\frac{F_G\,T}{V_G T_0}}{\lambda + \frac{HRTS_{GL}K_{MO}}{V_G} + \frac{F_G\,T}{V_G T_0} - \frac{\frac{HRTS_{GL}{}^2K_{MO}{}^2}{V_L V_G}}{\lambda + \frac{S_{GL}K_{MO}}{V_L}}} \quad \text{(toluene, ethyl acetate)} \quad \text{(S4)}$$

In a similar way, $\overline{E_c(t)}$ for ethyl trifluoroacetate or *n*-hexanal is given by Eq. S5 or S6, respectively, because E_L is 1 and $P_c(0) = C(0) = C_{diol}(0) = 0$.

$$\overline{E_{\mathrm{c}}(t)} = \frac{\frac{F_{\mathrm{G}}\,T}{V_{\mathrm{G}}T_0}}{\lambda + \frac{HRTS_{\mathrm{GL}}K_{\mathrm{MO}}}{V_G} + \frac{F_{\mathrm{G}}T}{V_{\mathrm{G}}T_0} - \frac{\frac{HRTS_{\mathrm{GL}}{}^2K_{\mathrm{MO}}{}^2}{V_{\mathrm{L}}V_{\mathrm{G}}}}{\lambda + \frac{S_{\mathrm{GL}}K_{\mathrm{MO}}}{V_{\mathrm{L}}} + k_{\mathrm{h}}}} \qquad \text{(ethyl trifluoroacetate)} \qquad \text{(S5)}$$

$$\overline{E_{\mathrm{c}}(t)} = \frac{\frac{F_{\mathrm{G}}\,T}{V_{\mathrm{G}}T_0}}{\lambda + \frac{HRTS_{\mathrm{GL}}K_{\mathrm{MO}}}{V_G} + \frac{F_{\mathrm{G}}T}{V_{\mathrm{G}}T_0} - \frac{\frac{HRTS_{\mathrm{GL}}{}^2K_{\mathrm{MO}}{}^2}{V_{\mathrm{L}}V_{\mathrm{G}}}}{\lambda + \frac{S_{\mathrm{GL}}K_{\mathrm{MO}}}{V_{\mathrm{L}}} + k_{\mathrm{f}} - \frac{k_{\mathrm{f}}k_{\mathrm{b}}}{\lambda + k_{\mathrm{b}}}}} \qquad (n\text{-hexanal}) \qquad \text{(S6)}$$

As seen in Eqs. S4–S6, $\overline{E_{\mathrm{c}}(t)}$ is independent on the input signal, $P_{\mathrm{in}}f(t)$. Therefore, for all of the test compounds in the present study, $E_{\mathrm{c}}(t)$ does not change if the input signal is changed.

Experimental determination of the convolution using the rectangular input pulse (Section 2.3.2)

The two PFA tubes each were connected to the two inlet ports and the two outlet ports, as shown in left schematic in Figure S2, when the gas mixture passed through the gas–liquid contactor. These inlet and outlet ports were placed on the upper side of the gas–liquid contactor. When the convolution of the RTD of the inlet region and the outlet region with the rectangular pulse was experimentally determined, the two tubes each were connected to each other as shown in right schematic in Figure S2. N_2 gas was additionally purged at a small rate of F_{g} (ca. 8×10^{-6} dm^3 s^{-1}), which rate was same as the rate of N_2 gas flowing through a hollow dead space between the contactor and the axis of the six-blade turbine to prevent the sample gas mixture from residing there, as described in Section 2.2.

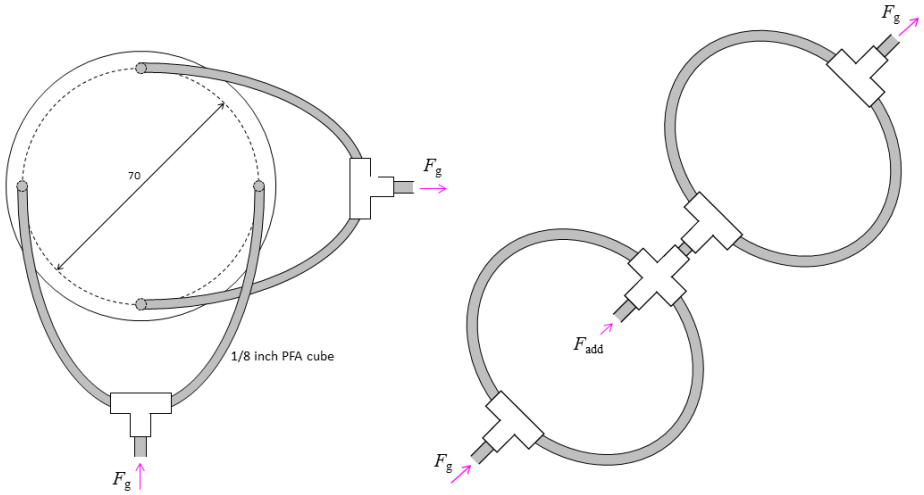

1098

1099 **Figure S2.** Connection of PFA tubes for the experimental runs in which the gas mixture passed
1100 through the gas–liquid contactor (left) and for determining the convolution (right). Number
1101 represents diameter in unit of mm.

1102

1103

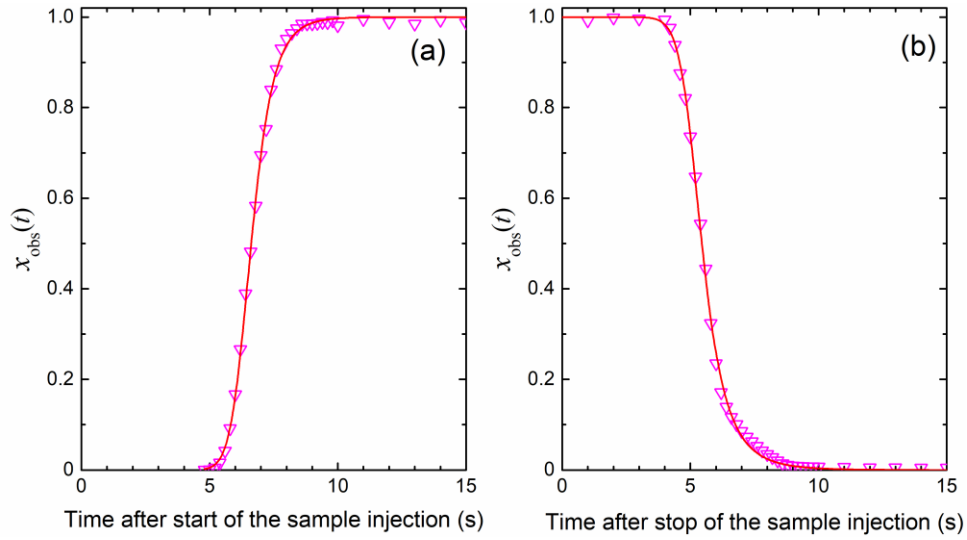

1104

1105 **Figure S3**. Time-profiles of $x_{obs}(t)$ for *n*-heptane after start (panel a) and stop (panel b) of
1106 injection by the sampling pump at 293.2 K.

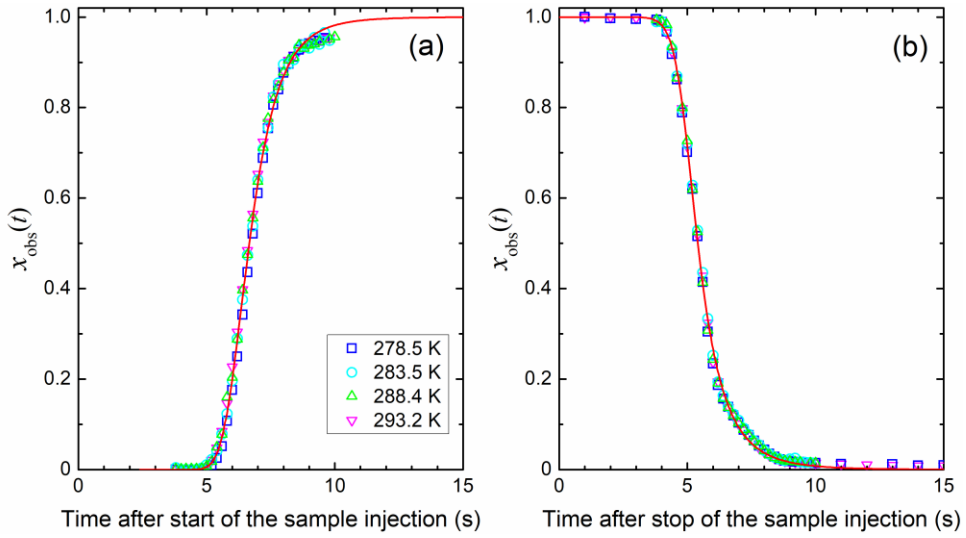

Figure S4. Time-profiles of $x_{obs}(t)$ for toluene after start (panel a) and stop (panel b) of injection by the sampling pump at each temperature.

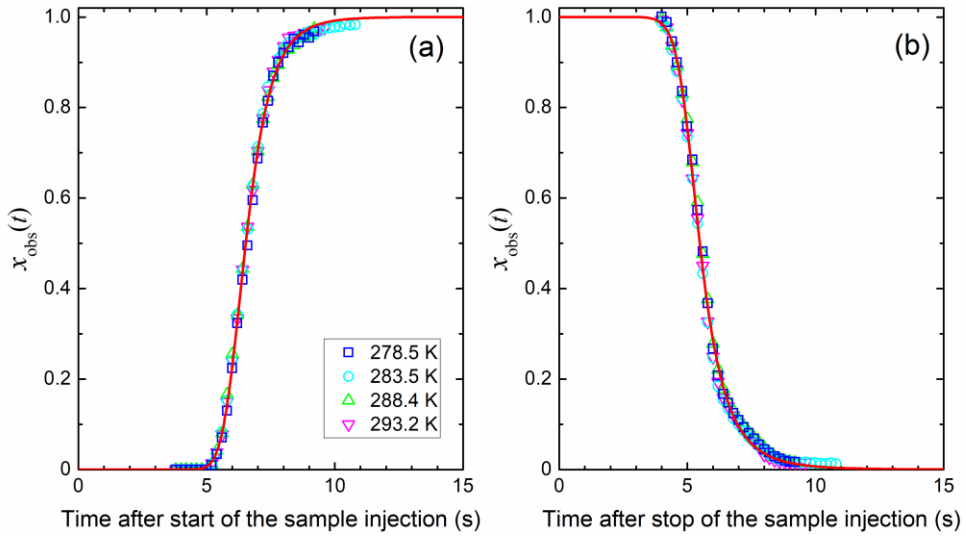

Figure S5. Time-profiles of $x_{obs}(t)$ for ethyl acetate after start (panel a) and stop (panel b) of injection by the sampling pump at each temperature.

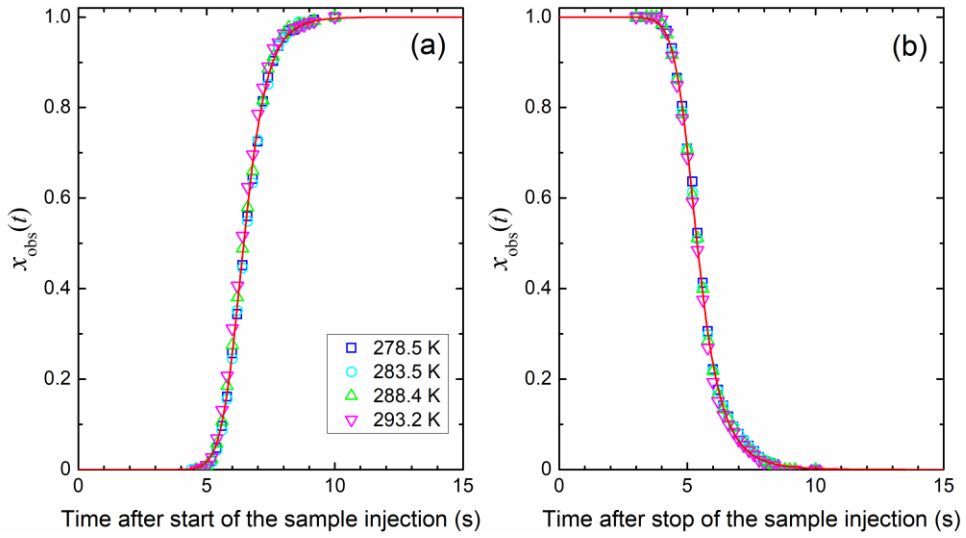

1115

1116 **Figure S6**. Time-profiles of $x_{obs}(t)$ for ethyl trifluoroacetate after start (panel a) and stop

1117 (panel b) of injection by the sampling pump at each temperature.

1118

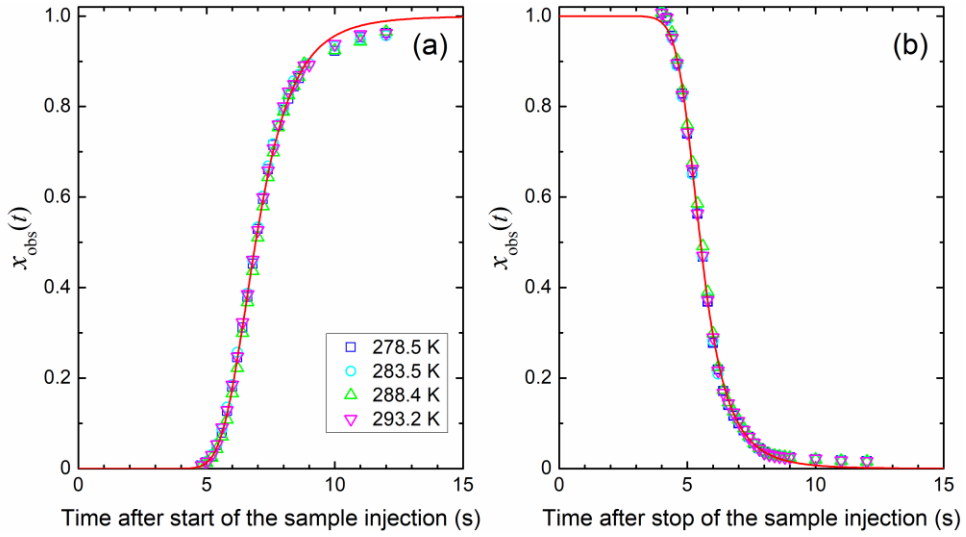

1119

1120 **Figure S7.** Time-profiles of $x_{obs}(t)$ for *n*-hexanal after start (panel a) and stop (panel b) of

1121 injection by the sampling pump at each temperature.

1122

1123 **Table S3.** Parameters determined from the experimental data (Figs S3–S7) by nonlinear

1124 regression with Eqs. 14 and 15.

	n-Heptane	Toluene	Ethyl acetate	Ethyl trifluoroacetate	*n*-Hexanal
a_1	6.3187	5.57294	5.77455	6.23037	5.77122
a_2	13.64045	9.16230	10.67952	12.99487	7.70174
a_3	1.6359	3.89802	2.88042	1.39610	3.10977
b_1	5.15333	4.98210	5.09565	5.14566	5.12048
b_2	−14.08338	−14.71308	−14.58990	−13.33461	−14.39817
b_3	0.59951	0.47260	0.50638	0.66994	0.51262

Table S4. Initial values set for the parameters in the first step, and the weighting errors, σ_{ij}, set in Eq. 22 in the second and third steps of the parameter-fitting procedure.

	Toluene	Ethyl acetate	Ethyl trifluoroacetate	*n*-Hexanal
H^{298} (M atm^{-1})	0.1	1	0.1	1
ΔH_{sol} (kJ mol^{-1})	−40	−40	−40	−40
k_h^{298} or k_f^{298} (s^{-1})	none	none	0.003	0.003
ΔE_{ah} or ΔE_{af} (kJ mol^{-1})	none	none	40	10
k_b^{298} (s^{-1})	none	none	none	0.003
ΔE_{ab} (kJ mol^{-1})	none	none	none	40
K_{MO} (dm s^{-1})	0.00001	0.00001	0.00001	0.00001
α_{corr}	1.0	1.0	1.0	1.0
σ_{ij}	0.002	0.001	0.002	0.0004

Table S5. Values of H, K_{MO}, and α_{corr} determined for toluene in deionized water by the parameter fitting in the simulation.

T (K)	H (M atm^{-1}) [a]	α_{corr} [a]	K_{MO} (10^{-4} dm s^{-1}) [a, b]
278.5	0.449 ± 0.004	0.920 ± 0.003	5.88 ± 0.05
			8.11 ± 0.07
			10.03 ± 0.10
283.5	0.346 ± 0.002	0.927 ± 0.002	6.60 ± 0.04
			8.79 ± 0.06
			12.87 ± 0.10
288.4	0.252 ± 0.001	0.923 ± 0.002	7.20 ± 0.05
			10.61 ± 0.07
			14.48 ± 0.11
293.2	0.199 ± 0.001	0.927 ± 0.002	8.63 ± 0.06
			11.36 ± 0.08
			16.28 ± 0.14

[a] Errors are at 90% confidence level for the parameter fitting in the simulation.

[b] The value at the top, middle or bottom in each row indicates the value of K_{MO} for deionized water stirred at 200, 300 or 400 rpm, respectively.

Table S6. Values of H, K_{MO}, and α_{corr} determined for ethyl acetate in deionized water by the parameter fitting in the simulation.

T (K)	H (M atm^{-1}) [a]	α_{corr} [a]	K_{MO} (10^{-4} dm s^{-1}) [a, b]
278.5	20.96 ± 0.58	0.869 ± 0.020	1.04 ± 0.01 1.19 ± 0.01 1.29 ± 0.02
281.0	17.09 ± 0.51	0.862 ± 0.022	1.24 ± 0.01 1.39 ± 0.02 1.50 ± 0.02
283.5	14.59 ± 0.43	0.862 ± 0.021	1.44 ± 0.01 1.62 ± 0.02 1.72 ± 0.02
286.0	12.80 ± 0.37	0.887 ± 0.022	1.71 ± 0.02 1.83 ± 0.02 1.99 ± 0.02
288.4	10.32 ± 0.26	0.873 ± 0.018	1.77 ± 0.01 2.02 ± 0.02 2.40 ± 0.02
290.8	9.23 ± 0.19	0.882 ± 0.015	2.13 ± 0.01 2.37 ± 0.01 2.65 ± 0.02
293.2	7.89 ± 0.22	0.882 ± 0.020	2.42 ± 0.02 2.76 ± 0.02 3.03 ± 0.02
295.7	7.05 ± 0.17	0.880 ± 0.017	2.76 ± 0.02 3.06 ± 0.02 3.42 ± 0.02

[a] Errors are at 90% confidence level for the parameter fitting in the simulation.

[b] The value at the top, middle or bottom in each row indicates the value of K_{MO} for deionized water stirred at 200, 300 or 400 rpm, respectively.

Table S7. Values of H, k_h, K_{MO}, and α_{corr} determined for ethyl trifluoroacetate in deionized water by the parameter fitting in the simulation.

T (K)	H (M atm^{-1}) [a]	k_f (10^{-3} s^{-1}) [a]	α_{corr} [a]	K_{MO} (10^{-4} dm s^{-1}) [a, b]
278.5	0.228 ± 0.003	1.05 ± 0.03	0.956 ± 0.006	6.54 ± 0.12 9.98 ± 0.18 11.45 ± 0.21
281.0	0.198 ± 0.002	1.22 ± 0.02	0.948 ± 0.005	7.10 ± 0.12 10.25 ± 0.17 11.35 ± 0.19
283.5	0.174 ± 0.003	1.37 ± 0.03	0.956 ± 0.006	7.32 ± 0.17 11.28 ± 0.25 12.44 ± 0.28
286.0	0.151 ± 0.002	1.60 ± 0.03	0.949 ± 0.005	7.95 ± 0.18 11.46 ± 0.25 12.49 ± 0.27
288.4	0.129 ± 0.002	1.86 ± 0.03	0.947 ± 0.004	7.78 ± 0.17 11.43 ± 0.24 13.98 ± 0.30
290.8	0.105 ± 0.002	2.03 ± 0.05	0.922 ± 0.004	8.29 ± 0.24 11.54 ± 0.32 14.78 ± 0.42
293.2	0.093 ± 0.002	2.30 ± 0.06	0.931 ± 0.005	9.01 ± 0.32 10.49 ± 0.37 15.39 ± 0.55
295.7	0.085 ± 0.002	2.69 ± 0.07	0.932 ± 0.004	8.38 ± 0.32 12.20 ± 0.46 14.84 ± 0.56

[a] Errors are at 90% confidence level for the parameter fitting in the simulation.

[b] The value at the top, middle or bottom in each row indicates the value of K_{MO} for deionized water stirred at 200, 300 or 400 rpm, respectively.

1148 **Table S8.** Values of H, k_h, K_{MO}, and α_{corr} determined for ethyl trifluoroacetate in 0.6 M aqueous
1149 NaCl by the parameter fitting in the simulation.

T (K)	H (M atm^{-1}) [a]	k_f (10^{-3} s^{-1}) [a]	α_{corr} [a]	K_{MO} (10^{-4} dm s^{-1}) [a, b]
278.5	0.171 ± 0.002	0.99 ± 0.02	0.960 ± 0.003	5.65 ± 0.09 8.46 ± 0.12 11.11 ± 0.16
281.0	0.145 ± 0.002	1.09 ± 0.03	0.948 ± 0.004	6.55 ± 0.13 9.07 ± 0.18 11.74 ± 0.23
283.5	0.131 ± 0.002	1.28 ± 0.03	0.953 ± 0.004	6.75 ± 0.14 9.48 ± 0.19 12.11 ± 0.24
286.0	0.105 ± 0.001	1.49 ± 0.04	0.938 ± 0.004	7.36 ± 0.17 10.57 ± 0.24 12.73 ± 0.29
288.4	0.097 ± 0.002	1.75 ± 0.05	0.959 ± 0.004	6.46 ± 0.20 10.15 ± 0.31 11.22 ± 0.34
290.8	0.079 ± 0.001	1.93 ± 0.06	0.944 ± 0.004	7.37 ± 0.26 10.31 ± 0.35 14.33 ± 0.49
293.2	0.069 ± 0.002	2.21 ± 0.08	0.932 ± 0.004	7.49 ± 0.37 10.98 ± 0.52 13.15 ± 0.63
295.7	0.063 ± 0.001	2.40 ± 0.08	0.938 ± 0.004	7.87 ± 0.37 11.08 ± 0.50 13.77 ± 0.63

1150 [a] Errors are at 90% confidence level for the parameter fitting in the simulation.

1151 [b] The value at the top, middle or bottom in each row indicates the value of K_{MO} for 0.6 M aqueous NaCl stirred at
1152 200, 300 or 400 rpm, respectively.

1153

Table S9. Values of H, K_{hyd}, k_f, K_{MO}, and α_{corr} determined for *n*-hexanal in deionized water by the parameter fitting in the simulation.

T (K)	H (M atm^{-1}) [a]	K_{hyd} [a]	k_f (10^{-3} s^{-1}) [a]	k_b (10^{-3} s^{-1}) [a]	α_{corr} [a]	K_{MO} (10^{-4} dm s^{-1}) [a, b]
278.5	7.94 ± 0.10	1.40 ± 0.07	1.11 ± 0.04	0.79 ± 0.02	0.919 ± 0.008	2.21 ± 0.03 2.46 ± 0.04 2.86 ± 0.04
281.0	6.56 ± 0.12	1.29 ± 0.08	1.25 ± 0.07	0.97 ± 0.03	0.939 ± 0.011	2.61 ± 0.05 2.94 ± 0.06 3.27 ± 0.07
283.5	5.62 ± 0.15	1.21 ± 0.11	1.40 ± 0.11	1.16 ± 0.05	0.936 ± 0.016	2.79 ± 0.09 3.42 ± 0.11 3.89 ± 0.12
286.0	4.83 ± 0.08	1.03 ± 0.06	1.47 ± 0.08	1.43 ± 0.04	0.953 ± 0.010	3.26 ± 0.07 3.65 ± 0.07 4.23 ± 0.09
288.4	4.03 ± 0.07	0.94 ± 0.06	1.62 ± 0.10	1.72 ± 0.05	0.945 ± 0.010	3.63 ± 0.08 4.21 ± 0.09 4.88 ± 0.11
290.8	3.57 ± 0.06	0.81 ± 0.06	1.68 ± 0.11	2.08 ± 0.06	0.950 ± 0.010	3.98 ± 0.09 4.65 ± 0.11 5.41 ± 0.12
293.2	3.09 ± 0.08	0.74 ± 0.08	1.82 ± 0.19	2.45 ± 0.11	0.945 ± 0.014	4.31 ± 0.15 5.18 ± 0.18 5.94 ± 0.21
295.7	2.69 ± 0.03	0.67 ± 0.03	1.98 ± 0.09	2.96 ± 0.06	0.989 ± 0.006	4.87 ± 0.07 5.77 ± 0.09 6.82 ± 0.10

[a] Errors are at 90% confidence level for the parameter fitting in the simulation.

[b] The value at the top, middle or bottom in each row indicates the value of K_{MO} for deionized water stirred at a speed of 200, 300 or 400 rpm, respectively.

Table S10. Values of H, K_{hyd}, k_f, K_{MO}, and α_{corr} determined for *n*-hexanal in 0.6 M aqueous NaCl by the parameter fitting in the simulation.

T (K)	H (M atm^{-1}) [a]	K_{hyd} [a]	k_f (10^{-3} s^{-1}) [a]	k_b (10^{-3} s^{-1}) [a]	α_{corr} [a]	K_{MO} (10^{-4} dm s^{-1}) [a, b]
278.5	6.11 ± 0.12	1.25 ± 0.10	1.10 ± 0.07	0.88 ± 0.04	0.936 ± 0.012	2.38 ± 0.06 2.97 ± 0.07 3.40 ± 0.08
281.0	5.13 ± 0.11	1.09 ± 0.09	1.12 ± 0.08	1.03 ± 0.05	0.908 ± 0.012	2.71 ± 0.07 3.40 ± 0.08 3.88 ± 0.10
283.5	4.25 ± 0.05	1.03 ± 0.05	1.31 ± 0.05	1.27 ± 0.03	0.912 ± 0.007	2.95 ± 0.04 3.81 ± 0.06 4.52 ± 0.07
286.0	3.67 ± 0.09	0.90 ± 0.09	1.46 ± 0.12	1.62 ± 0.07	0.932 ± 0.013	3.54 ± 0.10 4.24 ± 0.12 5.11 ± 0.15
288.4	3.20 ± 0.11	0.85 ± 0.12	1.56 ± 0.20	1.83 ± 0.11	0.953 ± 0.018	3.53 ± 0.15 4.89 ± 0.21 5.90 ± 0.26
290.8	2.78 ± 0.09	0.68 ± 0.10	1.57 ± 0.22	2.31 ± 0.14	0.924 ± 0.016	4.18 ± 0.17 5.12 ± 0.22 6.04 ± 0.26
293.2	2.37 ± 0.07	0.65 ± 0.09	1.83 ± 0.23	2.82 ± 0.14	0.925 ± 0.013	4.75 ± 0.18 6.05 ± 0.23 7.00 ± 0.27
295.7	2.08 ± 0.06	0.55 ± 0.08	1.90 ± 0.24	3.42 ± 0.17	0.953 ± 0.009	4.78 ± 0.17 5.35 ± 0.19 7.42 ± 0.27

[a] Errors are at 90% confidence level for the parameter fitting in the simulation.

[b] The value at the top, middle or bottom in each row indicates the value of K_{MO} for 0.6 M aqueous NaCl stirred at 200, 300 or 400 rpm, respectively.

Table S11. Values of H, K_{hyd}, k_f, K_{MO}, and α_{corr} determined for *n*-hexanal in 0.2 M aqueous Na_2SO_4 by the parameter fitting in the simulation.

T (K)	H (M atm^{-1}) [a]	K_{hyd} [a]	k_f (10^{-3} s^{-1}) [a]	k_b (10^{-3} s^{-1}) [a]	α_{corr} [a]	K_{MO} (10^{-4} dm s^{-1}) [a, b]
278.5	5.45 ± 0.07	1.40 ± 0.07	1.18 ± 0.05	0.85 ± 0.02	0.894 ± 0.006	2.33 ± 0.04 2.97 ± 0.05 3.51 ± 0.05
281.0	4.89 ± 0.12	1.19 ± 0.12	1.26 ± 0.10	1.05 ± 0.05	0.935 ± 0.014	2.71 ± 0.08 3.03 ± 0.09 3.87 ± 0.12
283.5	4.08 ± 0.05	1.14 ± 0.05	1.44 ± 0.06	1.27 ± 0.03	0.917 ± 0.007	3.01 ± 0.05 3.77 ± 0.06 4.51 ± 0.07
286.0	3.42 ± 0.09	1.03 ± 0.10	1.73 ± 0.15	1.68 ± 0.07	0.922 ± 0.013	3.52 ± 0.12 4.07 ± 0.14 5.04 ± 0.17
288.4	3.07 ± 0.08	0.90 ± 0.09	1.65 ± 0.15	1.84 ± 0.08	0.961 ± 0.012	3.51 ± 0.11 4.60 ± 0.15 5.62 ± 0.19
290.8	2.57 ± 0.07	0.82 ± 0.08	2.00 ± 0.18	2.44 ± 0.09	0.948 ± 0.013	4.30 ± 0.15 5.19 ± 0.17 6.40 ± 0.21
293.2	2.32 ± 0.05	0.68 ± 0.06	1.87 ± 0.16	2.77 ± 0.09	0.944 ± 0.006	3.49 ± 0.09 4.98 ± 0.13 6.15 ± 0.16
295.7	1.99 ± 0.10	0.56 ± 0.13	1.99 ± 0.44	3.57 ± 0.29	0.918 ± 0.013	4.46 ± 0.27 5.98 ± 0.37 6.74 ± 0.42

[a] Errors are at 90% confidence level for the parameter fitting in the simulation.

[b] The value at the top, middle or bottom in each row indicates the value of K_{MO} for 0.2 M aqueous Na_2SO_4 stirred at 200, 300 or 400 rpm, respectively.

Estimation of $\Delta G^{\ddagger}$ and $\Delta S^{\ddagger}$ of the hydration reaction of *n*-hexanal (Section 3.4)

According to absolute rate theory or transition state theory, k_f is given by Eq. S7:

$$k_f = \frac{k_B T}{h} \exp\left(-\frac{\Delta G^{\ddagger}}{RT}\right) \quad \text{(S7)}$$

where k_B is Boltzmann's constant; h is Planck's constant; $\Delta G^{\ddagger}$ is the free energy of activation. Letting the enthalpy, entropy, and volume of activation be $\Delta H^{\ddagger}$, $\Delta S^{\ddagger}$, and $\Delta V^{\ddagger}$, respectively, Eqs. S8 and S9 apply:

$$\Delta H^{\ddagger} = \Delta E_{af} + P\Delta V^{\ddagger} - RT \quad \text{(S8)}$$

$$\Delta G^{\ddagger} = \Delta H^{\ddagger} - T\Delta S^{\ddagger} \quad \text{(S9)}$$

The value of $\Delta G^{\ddagger}$ is calculated from the k_f^{298} value (Table 4) by using Eq. S7, and the value of $\Delta H^{\ddagger}$ is calculated form the ΔE_{af} value (Table 4) by using Eq. S8 and assuming that $P\Delta V^{\ddagger} \approx 0$. Then, the value of $\Delta S^{\ddagger}$ is calculated by using Eq. S9. Table S12 shows the calculation results for deionized water, 0.6 M aqueous NaCl, and 0.2 M aqueous Na_2SO_4 at 298.15 K.

Table S12. Values of $\Delta G^{\ddagger}$, $\Delta H^{\ddagger}$, $\Delta S^{\ddagger}$, and $-T\Delta S^{\ddagger}/\Delta G^{\ddagger}$ calculated at 298.15 K for the hydration reaction of *n*-hexanal in each aqueous phase.

Aqueous phase	$\Delta G^{\ddagger}$ (kJ mol^{-1}) [a]	$\Delta H^{\ddagger}$ (kJ mol^{-1}) [a]	$\Delta S^{\ddagger}$ (J mol^{-1} K^{-1}) [a]	$-T\Delta S^{\ddagger}/\Delta G^{\ddagger}$ [a]
Deionized water	88.25 ± 0.09	19.94 ± 1.86	−229 ± 6	0.774 ± 0.021
0.6 M aqueous NaCl	88.30 ± 0.23	20.77 ± 4.30	−227 ± 15	0.765 ± 0.049
0.2 M aqueous Na_2SO_4	88.03 ± 0.31	21.18 ± 5.66	−224 ± 19	0.759 ± 0.064

[a] Errors are at the 95% confidence level, with errors propagating only from those for the fitting (Table 4).

Estimation of D_G and D_L (Section 3.5)

Gas-phase diffusion coefficients of the test compounds in N_2 (D_G, in $dm^2\ s^{-1}$) and aqueous-phase diffusion coefficients of the test compounds (D_L, in $dm^2\ s^{-1}$) were estimated according to the equation by Fuller et al. (Eq. S10) [1, 2] and the correlation by Hayduk and Laudie (Eq. S11) [3], respectively.

$$D_G = \frac{1.0868 \times T^{1.75}}{\sqrt{m(A,B)}\left(\sqrt[3]{V_A}+\sqrt[3]{V_B}\right)^2} \times 10^{-2} \quad \text{(S10)}$$

$$D_L = \frac{13.26\times10^{-5}}{{\eta_2}^{1.4}{V_1}^{0.589}} \times 10^{-2} \quad \text{(S11)}$$

where m(A,B) is defined by Eq. S12; V_A is a diffusion volume of the sample (in cm^3) and V_B is that of N_2 (18.5 cm^3) [2]; η_2 is solution viscosity (in cps); V_1 is molar volume at normal boiling point for the sample; multiplication of 10^{-2} in the right side of each equation is a conversion factor for units.

$$m(\mathrm{A,B}) = \frac{2}{\frac{1}{m_A}+\frac{1}{m_B}} \quad \text{(S12)}$$

where m_A and m_B are the molecular weights (g mol^{-1}) of N_2 and the sample, respectively.

The values of V_A used in the calculation were 111.5, 94.3, 131.5, and 124.6 for toluene, ethyl acetate, ethyl trifluoroacetate, and *n*-hexanal, respectively. The values of V_1 used in the calculation were 118, 106, 119, and 123 for toluene, ethyl acetate, ethyl trifluoroacetate, and *n*-hexanal, respectively. The values of V_1 for toluene and ethyl acetate were referred to those in the literature [3], and those for ethyl trifluoroacetate and *n*-hexanal were approximated by molecular volume at ambient temperature. The calculated values of D_G and D_L for each sample at each temperature were listed in Table S13. These values of D_G and D_L were used for the

linear regression of the data with Eq. 35 and the estimate for k_{MG} and k_{ML} with Eqs. 32 and 33, respectively.

Table S13. Values of D_G and D_L calculated for each sample

T (K)	Toluene		Ethyl acetate		Ethyl trifluoroacetate		*n*-Hexanal	
	$10^4 D_G$ ($dm^2 s^{-1}$)	$10^8 D_L$ ($dm^2 s^{-1}$)	$10^4 D_G$ ($dm^2 s^{-1}$)	$10^8 D_L$ ($dm^2 s^{-1}$)	$10^4 D_G$ ($dm^2 s^{-1}$)	$10^8 D_L$ ($dm^2 s^{-1}$)	$10^4 D_G$ ($dm^2 s^{-1}$)	$10^8 D_L$ ($dm^2 s^{-1}$)
278.5	7.45	4.65	8.04	4.95	6.64	4.63	7.03	4.54
281.0	7.57	5.14	8.17	5.47	6.75	5.11	7.14	5.01
283.5	7.69	5.66	8.30	6.02	6.85	5.63	7.26	5.52
286.0	7.81	6.21	8.43	6.61	6.96	6.18	7.37	6.06
288.4	7.92	6.77	8.55	7.21	7.06	6.73	7.48	6.60
290.8	8.04	7.36	8.68	7.84	7.17	7.32	7.59	7.18
293.2	8.15	7.98	8.80	8.50	7.27	7.94	7.70	7.79
295.7	8.27	8.67	8.93	9.23	7.38	8.62	7.81	8.46

Table S14. Mass-transfer coefficients calculated of toluene, relative errors (RE) between the experimental and calculated values of K_{MO}, and percentage of resistance in the liquid phase (R_L).

T (K)	Stirring speed (rpm)	10^4 K_{MO} MODEL [a] (dm s^{-1})	RE (%)	10^4 k_{ML} [b] (dm s^{-1})	10^2 k_{MG} [c] (dm s^{-1})	R_L (%)
278.5	200	6.45	9.6	7.28	5.79	88.6
	300	8.73	7.6	10.2	6.19	85.5
	400	11.3	11.0	13.5	6.60	82.7
283.5	200	7.23	9.5	8.02	5.88	90.1
	300	9.83	11.9	11.3	6.28	87.4
	400	12.6	2.1	14.8	6.70	84.8
288.4	200	8.07	12.1	8.78	5.97	92.0
	300	11.0	4.0	12.3	6.38	89.7
	400	14.2	1.8	16.2	6.80	87.6
293.2	200	8.86	2.8	9.53	6.06	93.0
	300	12.2	7.0	13.4	6.47	91.0
	400	15.7	3.5	17.6	6.90	89.1

[a] Values are overall liquid-side mass-transfer coefficients between N_2 gas and deionized water which are calculated from the calculated values of k_{MG} (Eq. 32) and k_{ML} (Eq. 33) by using Eq. 31.

[b] Values are liquid-film mass-transfer coefficients in deionized water which are calculated using Eq. 33.

[c] Values are gas-film mass transfer coefficients in N_2 gas which are calculated using Eq. 32.

Table S15. Mass-transfer coefficients calculated of ethyl acetate between N_2 gas and deionized water, relative errors (RE) between the experimental and calculated values of K_{MO}, and percentage of resistance in the liquid phase (R_L).

T (K)	stirring speed (rpm)	10^4 K_{MO} MODEL [a] (dm s^{-1})	RE (%)	10^4 k_{ML} [b] (dm s^{-1})	10^2 k_{MG} [c] (dm s^{-1})	R_L (%)
278.5	200	1.08	3.1	7.51	6.02	14.3
	300	1.19	0.18	10.5	6.43	11.3
	400	1.30	0.70	13.9	6.86	9.3
281.0	200	1.29	3.5	7.89	6.06	16.3
	300	1.43	3.1	11.1	6.48	12.9
	400	1.56	4.2	14.6	6.91	10.7
283.5	200	1.48	2.7	8.28	6.11	17.9
	300	1.65	1.5	11.6	6.53	14.2
	400	1.81	5.3	15.3	6.96	11.8
286.0	200	1.66	2.9	8.68	6.16	19.1
	300	1.85	1.2	12.2	6.58	15.2
	400	2.04	2.2	16.1	7.02	12.7
288.4	200	1.98	12.1	9.06	6.20	21.9
	300	2.23	10.4	12.7	6.63	17.6
	400	2.47	2.7	16.8	7.07	14.7
290.8	200	2.18	2.3	9.45	6.25	23.1
	300	2.47	4.2	13.2	6.68	18.6
	400	2.73	2.8	17.5	7.12	15.6
293.2	200	2.48	2.6	9.84	6.29	25.2
	300	2.82	2.2	13.8	6.72	20.4
	400	3.13	3.1	18.2	7.17	17.2
295.7	200	2.72	1.5	10.3	6.34	26.6
	300	3.10	1.5	14.4	6.77	21.6
	400	3.46	0.92	19.0	7.23	18.2

[a] Values are overall liquid-side mass-transfer coefficients between N_2 gas and deionized water which are calculated from the calculated values of k_{MG} (Eq. 32) and k_{ML} (Eq. 33) by using Eq. 31.

[b] Values are liquid-film mass-transfer coefficients in deionized water which are calculated using Eq. 33.

[c] Values are gas-film mass transfer coefficients in N_2 gas which are calculated using Eq. 32.

Table S16. Mass-transfer coefficients calculated of ethyl trifluoroacetate, relative errors (RE) between the experimental and calculated values of K_{MO}, and percentage of resistance in the liquid phase (R_L).

T (K)	stirring speed (rpm)	10^4 K_{MO} MODEL [a] (dm s^{-1})	RE (%)	10^4 k_{ML} [b] (dm s^{-1})	10^2 k_{MG} [c] (dm s^{-1})	R_L (%)
278.5	200	6.79	3.8	7.26	5.47	93.5
	300	9.33	6.5	10.2	5.84	91.7
	400	12.1	5.5	13.4	6.23	89.9
281.0	200	7.18	1.1	7.63	5.51	94.1
	300	9.88	3.6	10.7	5.89	92.3
	400	12.8	12.8	14.1	6.28	90.7
283.5	200	7.56	3.3	8.00	5.55	94.5
	300	10.4	7.6	11.2	5.93	92.9
	400	13.5	8.8	14.8	6.33	91.4
286.0	200	7.96	0.14	8.39	5.60	95.0
	300	11.0	4.1	11.8	5.98	93.5
	400	14.3	14.4	15.5	6.38	92.1
288.4	200	8.36	7.5	8.76	5.64	95.5
	300	11.6	1.2	12.3	6.02	94.2
	400	15.0	7.6	16.2	6.43	92.9
290.8	200	8.78	5.9	9.13	5.68	96.1
	300	12.2	5.4	12.8	6.07	95.0
	400	15.9	7.3	16.9	6.47	93.8
293.2	200	9.17	1.8	9.51	5.72	96.4
	300	12.7	21.2	13.3	6.11	95.4
	400	16.6	7.9	17.6	6.52	94.3
295.7	200	9.57	14.1	9.91	5.76	96.6
	300	13.3	8.8	13.9	6.16	95.6
	400	17.3	16.8	18.3	6.57	94.6

[a] Values are overall liquid-side mass-transfer coefficients between N_2 gas and deionized water which are calculated from the calculated values of k_{MG} (Eq. 32) and k_{ML} (Eq. 33) by using Eq. 31.

[b] Values are liquid-film mass-transfer coefficients in deionized water which are calculated using Eq. 33.

[c] Values are gas-film mass transfer coefficients in N_2 gas which are calculated using Eq. 32.

Table S17. Mass-transfer coefficients calculated of *n*-hexanal, relative errors (RE) between the experimental and calculated values of K_{MO}, and percentage of resistance in the liquid phase (R_L).

T (K)	stirring speed (rpm)	10^4 K_{MO} MODEL [a] (dm s^{-1})	RE (%)	10^4 k_{ML} [b] (dm s^{-1})	10^2 k_{MG} [c] (dm s^{-1})	R_L (%)
278.5	200	2.17	2.2	7.19	5.63	30.1
	300	2.49	1.4	10.1	6.01	24.7
	400	2.79	2.4	13.3	6.41	21.0
281.0	200	2.51	4.0	7.55	5.67	33.2
	300	2.91	1.2	10.6	6.06	27.4
	400	3.27	0.19	14.0	6.46	23.4
283.5	200	2.82	0.97	7.93	5.72	35.5
	300	3.29	3.8	11.1	6.10	29.6
	400	3.72	4.3	14.7	6.51	25.3
286.0	200	3.15	3.3	8.30	5.76	37.9
	300	3.70	1.5	11.6	6.15	31.8
	400	4.20	0.57	15.4	6.56	27.3
288.4	200	3.57	1.4	8.67	5.80	41.2
	300	4.23	0.68	12.2	6.20	34.8
	400	4.84	0.82	16.0	6.61	30.2
290.8	200	3.90	2.0	9.04	5.84	43.1
	300	4.64	0.30	12.7	6.24	36.6
	400	5.32	1.6	16.7	6.66	31.8
293.2	200	4.30	0.18	9.42	5.89	45.7
	300	5.16	0.47	13.2	6.29	39.0
	400	5.94	0.17	17.4	6.71	34.1
295.7	200	4.72	3.2	9.81	5.93	48.1
	300	5.69	1.4	13.8	6.33	41.4
	400	6.60	3.2	18.2	6.76	36.3

[a] Values are overall liquid-side mass-transfer coefficients between N_2 gas and deionized water which are calculated from the calculated values of k_{MG} (Eq. 32) and k_{ML} (Eq. 33) by using Eq. 31.

[b] Values are liquid-film mass-transfer coefficients in deionized water which are calculated using Eq. 33.

[c] Values are gas-film mass transfer coefficients in N_2 gas which are calculated using Eq. 32.

REFERENCES

[1] E.N. Fuller, P.D. Schettler, J.C. Giddings, 1966. NEW METHOD FOR PREDICTION OF BINARY GAS-PHASE DIFFUSION COEFFICIENTS, Industrial & Engineering Chemistry 58, 18-27.

[2] M.J. Tang, R.A. Cox, M. Kalberer, 2014. Compilation and evaluation of gas phase diffusion coefficients of reactive trace gases in the atmosphere: volume 1. Inorganic compounds, Atmospheric Chemistry and Physics 14, 9233-9247.

[3] W. Hayduk, H. Laudie, 1974. Prediction of diffusion coefficients for nonelectrolytes in dilute aqueous solutions, AlChE J. 20, 611-615.